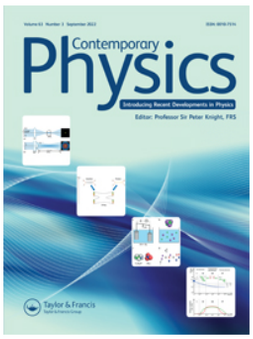

Contemporary Physics

ISSN: 0010-7514 (Print) 1366-5812 (Online) Journal homepage: www.tandfonline.com/journals/tcph20

Interstellar objects

Darryl Z. Seligman & Amaya Moro-Martín

To cite this article: Darryl Z. Seligman & Amaya Moro-Martín (2022) Interstellar objects, Contemporary Physics, 63:3, 200-232, DOI: 10.1080/00107514.2023.2203976

To link to this article: https://doi.org/10.1080/00107514.2023.2203976

Published online: 22 May 2023.

CONTEMPORARY PHYSICS
2022, VOL. 63, NO. 3, 200–232
https://doi.org/10.1080/00107514.2023.2203976

Taylor & Francis
Taylor & Francis Group

Interstellar objects

Darryl Z. Seligman[a] and Amaya Moro-Martín[b,c]

[a]Department of Astronomy and Carl Sagan Institute, Cornell University, Ithaca, NY, USA; [b]Space Telescope Science Institute, Baltimore, MD, USA; [c]Department of Physics and Astronomy, Johns Hopkins University, Baltimore, MD, USA

ABSTRACT

Since 2017, two macroscopic interstellar objects have been discovered in the inner Solar System, both of which are distinct in nature. The first interstellar object, 1I/'Oumuamua, passed within ∼63 lunar distances of the Earth, appeared asteroidal lacking detectable levels of gas or dust loss, yet exhibited a nongravitational acceleration. 1I/'Oumuamua's brief visit left open questions regarding its provenance which has given rise to many theoretical hypotheses, including an icy comet lacking a dust coma, an elongated fragment of a planet or planetesimal that was tidally disrupted, and an ultra-porous fractal aggregate. The second interstellar object, 2I/Borisov, was distinct from 1I/'Oumuamua in terms of its bulk physical properties and displayed a definitive cometary tail. We review the discoveries of these objects, the subsequent observations and characterisations, and the theoretical hypotheses regarding their origins. We describe 1I/'Oumuamua and 2I/Borisov in the context of active asteroids and comets in the Solar System. The discovery of these two objects implies a galactic-wide population of $\sim 10^{26}$ similar bodies. Forthcoming observatories should detect many more interstellar planetesimals which may offer new insights into how planetary formation processes vary throughout the Galaxy.

ARTICLE HISTORY
Received 24 February 2023
Accepted 13 April 2023

KEYWORDS
Interstellar objects; comets; asteroids; meteoroids; planetary systems: formation; protoplanetary disks; circumstellar disks; dynamical evolution and stability; Solar System: formation; Oort cloud; galaxy: local interstellar matter

1. Comets in the solar system

1.1. Historical perspective

For hundreds of years prior to the discovery of 1I/'Oumuamua and 2I/Borisov, astronomers had predicted that the Galaxy would be filled with icy bodies ejected from extrasolar planetary systems. Therefore, the existence of small bodies of extrasolar provenance observed passing through our own Solar System on hyperbolic trajectories was not inherently surprising. A full detailed account of the historical perspective on cometary science can be found in [1] including a discussion of interstellar comets.

As early as 1705, Edmond Halley considered the hypothesis that some comets arrived from interstellar space [2]. Halley computed the orbits of 24 comets and demonstrated that none of them had distinctly hyperbolic trajectories – outlined in the Table captioned *The astronomical elements of the motions in a parabolick orb of all the Comets that have been hitherto duly observ'd*. He therefore concluded that the population of detected comets at the time had all formed within the Solar System. Immanuel Kant further postulated that comets formed from diffuse nebular material at large heliocentric distances but were still gravitationally bound to the Sun [3].

On the other hand, the Italian astronomer Giuseppe (translated in English to Joseph) Lagrange argued that the high eccentricities and inclinations of cometary orbits were incompatabile with the nebular hypothesis. Although he believed that comets formed within the Solar System, he showed that their orbits could be produced by catastrophic disruption events from impacts with planets. Lagrange argued that his calculations, in combination with the nebular hypothesis, explained the entire census of celestial objects within the Solar System [4].

In 1812, William Herschel obtained detailed observations of two comets, both of which attained different brightness levels despite similar perihelia distances. He outlined these findings in two papers published in 1812: 'Observations of a Comet, with Remarks on the Construction of Its Different Parts' and 'Observations of a Second Comet, with Remarks on Its Construction' [5,6]. The brightness differences led him to speculate that some comets may originate beyond the Solar System, and that the variable activity levels could be attributed to the accumulation of matter in interstellar space:

CONTACT D. Z. Seligman dzs9@cornell.edu

> Should the idea of age be rejected, we may indeed have recourse to another supposition, namely, that the present comet, since the time of some former perihelion passage, may have acquired an additional quantity (if I may so call it) of unperihelioned matter, by moving in a parabolical direction through the immensity of space, and passing through extensive strata of nebulosity.

In 1813, Pierre-Simon de Laplace offered an alternative hypothesis to that of Lagrange [7]. He argued that the eccentricities and inclinations of comets could be explained if they originated from interstellar space, echoing the hypothesis of William Herschel:

> Among the hypotheses that have been proposed on the origin of comets, the most probable seems to me to be that of Mr. Herschel, which consists in looking at them as small nebulae formed by the condensation of the nebulous matter diffused with such profusion in the universe Comets.

Laplace believed that comets formed via the condensation of nebular material throughout the Galaxy and subsequently travelled from stellar system to system. He calculated that 1/5713 comets within a 100,000 au sphere around the Sun would exhibit perihelia <2 au with strongly hyperbolic trajectories. He concluded that the majority of interstellar comets would reach the Earth on parabolic orbits, consistent with the distribution of cometary orbits observed at that time. Unfortunately, Laplace neglected to include the proper motion of the Sun with respect to the galactic motion in his calculations. Herschel had speculated that the sun moved with respect to other stars in the Milky Way after observing the motion of several nearby stars decades previously [8].

It was not until 1866 and 1867 that Giovanni Schiaparelli redid the calculations from Laplace while including the proper Solar motion. He demonstrated that the trajectories of interstellar comets would almost entirely be significantly hyperbolic. Therefore, while provocative in nature, the claim that interstellar comets were regularly seen throughout the Solar System was largely disregarded.

1.2. Long and short period comets

The comets in the Solar System are broadly categorised into two families: the Long Period Comets (LPCs) and the Short Period Comets (SPCs), the latter of which are commonly referred to as ecliptic comets or Jupiter Family Comets (JFCs). The LPCs arrive uniformly across the sky with an isotropic distribution of inclinations. This was attributed to an isotropic cloud of comets as the source region of the LPCs, referred to as the Oort cloud [9]. The Oort cloud spans 50,000 au and, based on the occurrence of LPCs, it has been estimated to contain 10^{11}–10^{12} km-sized Oort cloud objects [10–12]. The total mass of the Oort cloud is typically quoted as 1 Earth mass ($M_\oplus$), but up to 20 $M_\oplus$ is allowable by the current data [13].

Meanwhile, the tendency for the SPCs – with orbital periods <200 years – to lie within the ecliptic plane with low typical inclinations implies that these objects come from a different source region than the Oort cloud [14–18]. It was therefore hypothesised that there existed a reservoir of icy objects past Neptune that sourced the SPCs. A small fraction of these trans-Neptunian objects would be gravitationally perturbed onto trajectories interior to the orbit of Neptune. Subsequent dynamical interactions with the giant planets would transfer some of these objects into the inner Solar System [19–27]. This trans-Neptunian population was verified in 1993 with the discovery of the first Kuiper belt object (KBO) (other than Pluto) [28]. Thousands of trans-Neptunian objects have since been identified and characterised [29–33]. It is now widely accepted that the JFCs are transported into the inner Solar System via the Centaur region between the giant planets [34–41].

1.3. Ejection of interstellar comets by the solar system

The existence of the Kuiper belt and Oort cloud has led to the realisation that the Solar System underwent a period of planetary migration. The migration of the giant planets specifically would have scattered a large amount of debris to large heliocentric distances, thereby populating the Kuiper belt and Oort cloud. There are varying hypotheses regarding the details of the planetary migration in the early Solar System. For a recent review of different formation models, we refer the reader to [42].

Some authors have claimed that the Solar System underwent a transient period of violent dynamical instability in a model which is colloquially referred to as the 'Nice model' [43,44]. Numerical experiments of this instability have demonstrated that it would have generated $\sim 30 M_\oplus$ of material in interstellar comets. More general giant planet driven migration could also eject a similar amount of material [45,46].

The majority of this material would be ejected in the form of interstellar comets. However, a fraction that has been estimated to be between 1% and 10% remained in the Solar System due to the effect of galactic tides and stellar flybys. These objects, now protected from further interactions with the giant planets and from gravitational ejection, remain bound with eccentricity $e < 1$ [12,45,47,48]. These processes likely generated the present day Kuiper belt and Oort cloud.

1.4. Cometary outgassing

Comets within the Solar System are generally detected via their distinct and explosive coma – the gas surrounding the nucleus – along with dusty cometary tails. These coma form when solar radiation received at the surface of the comet produces an outflow of gas and dust. The energy from the solar irradiation first powers the phase transition of the surface or subsurface ice into gas in a process called sublimation. Next, the radiation energy is converted into kinetic energy which heats the gas to the thermal speed to power the outflowing jet. Dust particles and debris that are either residing on the surface of the comet or trapped within the ice typically travel along with the gas in the outflow. This entire process produces a cometary outflow and the dusty tail that, in some cases, is detectable from Earth. Solar photons are then reflected off of the surface of these dust grains, which gives rise to the beautiful cometary tails. The wavelengths of light that are reflected depend on the size of the dust grains. For example, optical photons are reflected by $\sim$ micron-sized dust grains. This dust production can make the comet orders of magnitude brighter.

This mass loss produces a recoil effect on cometary nuclei [49,50]. The force of the outflowing material can produce a nongravitational acceleration of the nucleus, typically written as $\vec{\alpha}_{ng}$. A formalism to describe the nongravitational accelerations of comets was introduced by [51] as

$$\vec{\alpha}_{\rm ng} = \left(\underbrace{A_1\hat{\mathbf{r}}}_{\rm Radial} + \underbrace{A_2\hat{\mathbf{t}}}_{\rm Transverse} + \underbrace{A_3\hat{\mathbf{n}}}_{\rm Out-of-plane} \right) \underbrace{g(r_H)}_{\rm Radial\ dependance} . \quad (1)$$

In Equation (1), $\hat{\mathbf{r}}$, $\hat{\mathbf{t}}$, $\hat{\mathbf{n}}$ are the radial, transverse and out-of-plane directions with respect to the orbit of the comet. The $g(r_H)$ function, or Marsden function, is a function that parametrises the dependence on the heliocentric distance r_H. The magnitudes of the three components of the acceleration are A_1, A_2 and A_3, normalised to a heliocentric distance of $r_H = 1$ au.

This recoil acceleration is related to the amount of mass lost in the outflow, written as $\mathrm{d}M/\mathrm{d}t$ with speed V_s. If the outflow is perfectly collimated in one direction – typically thought to be normal to the surface – the outflow imparts momentum in one direction. If the outflow is completely isotropic, then the change of momentum perfectly cancels. We parametrise the degree of collimation in the outflow with the parameter k_R, where $k_R = 1$ and $k_R = 0$ correspond to the collimated and isotropic cases, respectively. Realistically, cometary outflows are somewhere between these two extremes and $0 < k_R < 1$. Assuming that the comet has a spherical nucleus with radius r_n and bulk density $\rho_{\rm bulk}$, the mass loss can be written as

$$\frac{\mathrm{d}M}{\mathrm{d}t} = \left(\underbrace{4\pi r_n^3 \rho_{\rm bulk} / 3}_{\rm Mass\ of\ Nucleus} \right) \left(\underbrace{|\vec{\alpha}_{ng}| / k_R V_s}_{\rm Rate} \right) . \quad (2)$$

The velocity of the outgassing species is related to the thermal speed. For example, H_2O ice interior to 2 au has a sublimation temperature $T \sim 200$ K which corresponds to a velocity $V_s \sim 500\ \mathrm{m\,s^{-1}}$. This effect has been measured on a subset of comets in the Solar System. In Figure 1, we show measured nongravitational accelerations of Short and Long Period Comets.

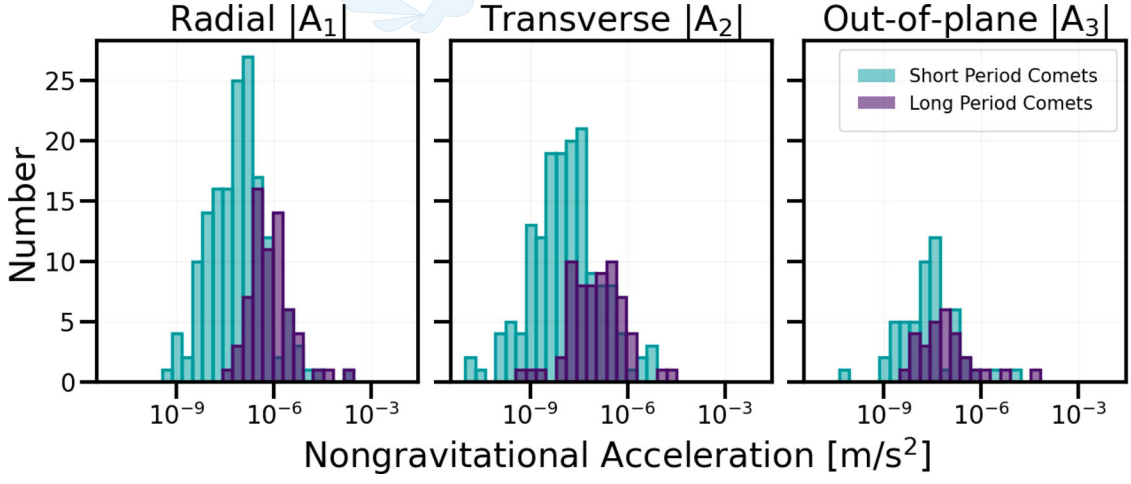

Figure 1. The measured nongravitational accelerations of Short-Period Comets (teal) and Long-Period Comets (purple). The three panels show the radial (left), transverse (middle) and out-of-plane (right) components of measured accelerations. Nongravitational accelerations are taken from the JPL Small Body Database.

1.5. Composition of comets

Cometary tails are typically observed in optical wavelengths via the reflection of solar photons off of micron-sized dust particles in the outflows. However, emission and absorption of photons through the gas coma can also be measured spectroscopically, providing a direct probe of the *volatile* content of the coma. Therefore, the composition of the sublimating gas itself in the coma has been directly measured in many cases. This volatile composition can be related to the bulk composition of the comet, with the caveat that it only represents the species active at the time of the observation. Subsurface or inactive surface ices of other species may be present in the nucleus but not the coma, thereby evading detection at any given point during an apparition.

Despite these complications, the volatile content of a large set of comets has been measured. The majority of comets consist primarily of H_2O ice [52–56]. The next two most abundant volatiles in comets are CO_2 and CO [56]. Other carbon and nitrogen species can be abundant as well including CH_4, C_2H_2, C_2H_6, CH_3OH, NH_3 and HCN (see figure 2 in [57]). In Figure 2, we show typical compositions of carbon enriched and carbon depleted Solar System comets.

The composition of a comet can be linked to its formation location within the protoplanetary disk that initially formed from the Solar nebulae. The temperature of the ambient gas in the disk decreases with increasing distance from the Sun. Therefore, certain volatile species only freeze onto dust grains exterior to a characteristic temperature front, or snowline. For example, it is believed that in the protosolar disk, H_2O and CO were frozen exterior to the current day orbits of Jupiter and Neptune, respectively. An overview of cometary composition measurements, including measured production rates of CO, CO_2 and H_2O, was provided by [61]. Based on the lack of hypervolatiles detected in the coma of most comets, they argued that the majority of comets formed in the giant planet region, where these hypervolatiles would not exist as ices to be incorporated into comets. The *Akari* spacecraft provided a homogeneous survey of CO_2, CO and H_2O production rates in Solar System comets [60]. This provides a further line of evidence that the Kuiper belt and Oort cloud objects formed at closer heliocentric distances and were subsequently scattered outwards. However, it is important to note that this simplified picture does not incorporate the, potentially significant, post-formation processing that also removes volatiles and hypervolatiles from comets.

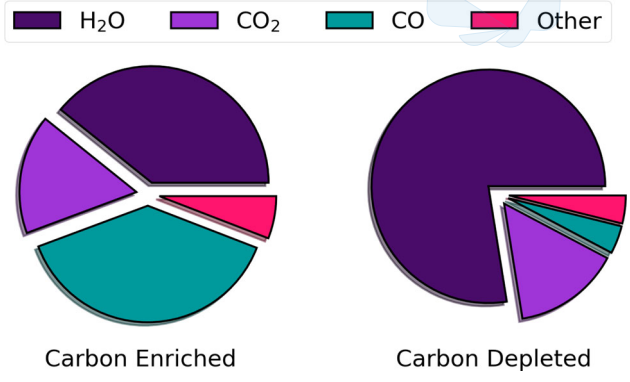

Figure 2. The typical compositions of carbon enriched and depleted Solar System comets. This is a generalised version of an analogous figure in [58] and adapted from [59]. The carbon depleted comet is representative of many of the Solar System comets for which production rate measurements of CO_2, CO and H_2O exist (see table 1 in [59]). The carbon enriched comet is C/2006 W3 Christensen [60].

2. 1I/'Oumuamua

2.1. Discovery

The first interstellar object was discovered by Robert Weryk on 2017 October 19 from Haleakalā on Maui, Hawaii [62]. It was identified during the course of typical operations of the Pan-STARRs project [63], a NASA funded all-sky survey optimised for detecting small Solar System bodies. The survey uses two 1.8-m telescopes and associated gigapixel detectors on the summit of Haleakalā. It is sensitive to a limiting magnitude of $V = 22$ and produces nightly images that have $\sim$6000 deg^2 resolution.

The object was initially flagged as a potentially hazardous near-Earth object (NEO) – a population of small bodies from the asteroid belt that have been gravitationally perturbed onto Earth crossing trajectories. After only a few days of intensive and globally coordinated follow-up observations, the orbit of the object was confirmed to be hyperbolic with an eccentricity $e = 1.198$. The possibility that it was a Solar System object that had been gravitationally perturbed onto an unbound trajectory was quickly ruled out [64,65]. The hyperbolic trajectory therefore confirmed that the object could not have originated from within our Solar System and definitively formed elsewhere. It was discovered when it was $\sim$63 lunar distances from the Earth, after it had reached its closest approach to the Sun on 2017 September 9 and as it was rapidly departing the Solar System. The object had a closest approach distance to the Sun of $q \sim 0.255$ au and inclination $i = 122.8^\circ$.

There was explosive interest in the object after it was announced to be interstellar, both from the scientific community and from the general public. Due to its close proximity to the Earth and its resulting rapid sky motion,

the object was only observable for ∼4 weeks with ground based telescopes. There was a global scramble to observe the rapidly moving object and director discretionary time was awarded to observe it on many major telescopes. The last successful ground based observation of the object was on 2017 November 21. In the following section, we review all of the measurements obtained of the rapidly fading object. For recent reviews, see [66,67].

2.2. Observations

Immediately following the announcement of the discovery of the object, [69] obtained the first optical spectrum reflected from its surface on 2017 October 25 with the Palomar 5-m Hale telescope. The spectrum spanned from 520 to 950 nm and was entirely featureless with a reddened slope. Further imaging and spectroscopic observations were taken of 1I/'Oumuamua the following night with the same telescope that indicated a consistently reddened surface colour [70].

In a paper often credited with the discovery of 1I/'Oumuamua, [71] reported time resolved photometric observations of the object from the nights of 2017 October 25, 26 and 27. These observations included 3.5 h on the Very Large Telescope (VLT) 8-m telescope, 3.5 h on Gemini south, 3 h on the Keck 10-m telescope, 9 h on the United Kingdom Infrared Telescope (UKIRT), and 8 h on the Canada–France–Hawaii telescope (CFHT). Deep stacks of the images showed no evidence of cometary activity or dust tail.

In [68], observations were reported on the nights of 2017 October 25, 26, 29 and 30 with the 2.5-m diameter Nordic Optical Telescope (NOT) and 4.5 h on the WIYN telescope, located at Kitt Peak National Observatory in Arizona. They measured the optical colours of the nucleus to be B-V $= 0.70 \pm 0.06$, V-R $= 0.45 \pm 0.05$ and found a lack of micron-sized dust particles. Figure 3 shows an image of 1I/'Oumuamua taken with the NOT telescope, clearly lacking a dust tail and apparent coma.

Spectroscopic observations of 1I/'Oumuamua were reported in [72], with data from the 4.2-m William Herschel Telescope (WHT) on La Palma on 2017 October 25 and the X-shooter spectrograph located at the European Southern Observatory 8.2 m Very Large Telescope (VLT) on 2017 October 27. The resulting spectrum covered 0.3–2.5 μm, and was also featureless and reddened. Photometric observations (8.06 h) were reported by [73] obtained with the Gemini North 8.1-m telescope on 2017 October 27 and 28 with extremely high temporal cadence, resulting in 431 r'-band images. Additional spectroscopic observations were described by [74] obtained with the Gemini telescope (2 h) and the 4.2 m

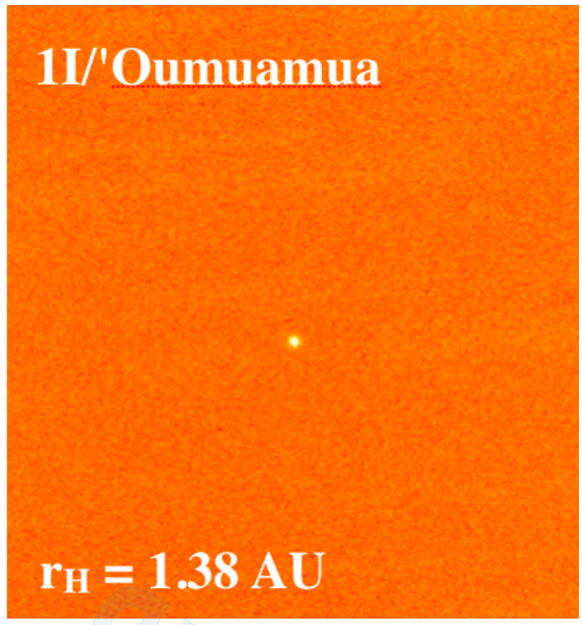

Figure 3. An image of 1I/'Oumuamua taken with the 2.5 m Nordic Optical Telescope on 2017 October 26. The object displays no distinct cometary tail. In the figure, r_H corresponds to the heliocentric distance of the object when the image was taken. This figure has been reproduced from [68].

William Herschel Telescope (WHT) (2 h), on 2017 October 29 and 30, respectively. One those same dates, [75] obtained observations (4 h) using the Apache Point Observatory (APO) ARCTIC camera on the 3.5-m telescope (2017 October 29) and [76] obtained photometric data (2.8 h) with the Lowell Observatory 4.3-m Discovery Channel Telescope (DDT) (2017 October 30).

The NASA/ESA *Hubble Space Telescope* (HST) allotted 9 orbits of time to monitor 1I/'Oumuamua. These data were taken with the UVIS channel from the Wide-Field Camera 3 (WFC3) using the F350LP filter. These observations occurred during 2017 November, December and 2018 January over all 9 orbits. Photometric brightness variations were reported during 2017 November 21 and 22, and the remaining observations provided astrometric measurements as well [77]. They also presented data in the same paper with the CFHT MegaCam imager from 2017 November 22 and 23 and the Magellan-Baade 6.5-m telescope at Las Campanas Observatory from 2017 November 21, 22 and 23. They compiled a composite light curve over a 29.3 day period spanning about 0.13 au of the trajectory containing a total of 818 photometric observations of the object reported by [68,71,73–78].

In addition to these detections of 1I/'Oumuamua, several attempts to observe the object resulted in non-detections. Some of these provided critical upper limits on the production rates of dust and certain volatile species. [70] attempted to observe 1I/'Oumuamua with

Table 1. Summary of all measured upper limits on production rates of various volatile species and dust from 1I/'Oumuamua.

Species	Physical property	Value	Distance	Reference
CN	Q(CN)[mol s^{-1}]	$<2 \times 10^{22}$	1.4 au	[70]
C_2	Q(C_2)[mol s^{-1}]	$<4 \times 10^{22}$	1.4 au	[70]
C_3	Q(C_3)[mol s^{-1}]	$<2 \times 10^{21}$	1.4 au	[70]
OH	Q(OH)[mol s^{-1}]	$<1.7 \times 10^{27}$	1.8 au	[79]
CO_2	Q(CO_2)[mol s^{-1}]	$<9 \times 10^{22}$	2.0 au	[80]
CO*	Q(CO)[mol s^{-1}]	$<9 \times 10^{21}$	2.0 au	[80]
CO	Q(CO) [mol s^{-1}]	$<9 \times 10^{23}$	2.0 au	[81]
Dust	Q(Dust)[kg s^{-1}]	$<1.7 \times 10^{-3}$	1.4 au	[71]
Dust	Q(Dust)[kg s^{-1}]	$<2 \times 10^{-4}$	1.4 au	[68]
Dust	Q(Dust)[kg s^{-1}]	<10	1.4 au	[70]

Notes: Note that the measurement indicated with * had a typographical error which was later fixed.

the Canadian Meteor Orbit Radar, and the non-detection provided upper limits on the production of CN, C_2 and C_3 (Table 1). An upper limit on the production rate of OH via the OH 18-cm line (Table 1) were reported by [79] based on 4 h of observations with the Green Bank Telescope on 2017 November 12.

The *Spitzer Space Telescope* observed 1I/'Oumuamua for 32.6 h on 2017 November 21 and 22. These observations were taken with the 4.5 μm band in the IRAC channel 2, which would have detected fluorescence of carbon-based molecules such as CO or CO_2. However, these observations resulted in a non-detection which provided an upper limit on the production of CO and CO_2 of the object [80] (Table 1). Note that the production of CO contained a typographical error and was later corrected by [81].

A precovery of 1I/'Oumuamau prior to perihelion from 2017 September was attempted by [82]. Their search for the object in extant data from Solar TErrestrial RElations Observatory (STEREO) and the Solar and Heliospheric Observatory (SOHO) resulted in nondetections.

Several teams attempted to detect radio signal from 1I/'Oumuamua, all of which were unsuccessful. Data were obtained with the Robert C. Byrd Green Bank Telescope beginning on 2017 December 13 [83], the Murchison Widefield Array (MWA) on 2017 November 28 [84] and the Allen Telescope Array from 2017 November 23 through December 5 [85]. All of these upper limits on production rates are summarised in Table 1.

2.3. Nucleus properties

2.3.1. Size

The size of asteroids can be related to their absolute magnitude [86] with the following relationship:

$$2\left(\frac{r_{\rm n}}{1\,{\rm km}}\right) = \left(\frac{1329}{\sqrt{p}}\right) 10^{-0.2\,H}. \qquad (3)$$

In Equation (3), H is the absolute magnitude inferred from the brightness and geometry of the orbit ($H = 22.4$ for 1I/'Oumuamua), p is the geometric albedo and $r_{\rm n}$ is the radius in kilometres of the assumed to be spherical nucleus. For the case of asymmetrical shaped objects, $r_{\rm n}$ is estimated as the effective radius. This is approximated as the circular cross-section of an ellipse with aspect ratio a:b, and therefore $r_{\rm n} = (ab)^{1/2}$. The albedo is a measure of the fraction of light reflected off of the surface versus absorbed. The albedo of nitrogen ice seen on the surface of Pluto can be as high as $p = 0.8--0.9$, while H_2O ice on the surface of Charon has a more moderate albedo $p \sim 0.25$ [87]. However, the albedos of carbonaceous surfaces of asteroids are much smaller with $p \sim 0.04$.

The surface composition of 1I/'Oumuamua is unconstrained and therefore the exact size of the object is not known. Literature estimates of the size varied from 55 m [68], 70 ± 3 m [71], 80 m [73] to 114 m [76]. Assuming an albedo $p = 0.1$, [66] estimated an effective radius of 80 m. This value is consistent with the nuclear radius calculated with Equation (3) using an absolute magnitude of $H = 22.4$.

2.3.2. Colours

The surface colours of small bodies can be measured spectroscopically. These colours do not give definitive information of the surface compositions but can be used to identify surface features. For example, asteroids in the inner Solar System have reddish colours that are due to iron produced by particle bombardment.

Most objects in the Solar System have slightly reddened reflectance spectra, with the exception of cold classical KBOs and some Centaurs. The inclination distribution of the classical KBOs is known to be bimodal. Objects with low inclinations $i < 5^\circ$ are referred to as the cold classical KBOs, while objects with larger inclinations are hot classical KBOs [88,89]. The cold classical KBOs likely formed in situ and therefore have little or no residency time in the inner Solar System [42]. These cold classical KBOs and some inactive Centaurs have surface reflectance spectra consistent with 'ultra-red' material [90–92]. It is believed that the ultra-red material is caused by carbon compounds that are unstable and depleted in the warmer inner Solar System, and produced via space weathering from cosmic rays and interstellar medium (ISM) plasma [68].

Therefore, a natural hypothesis is that the surface colours of interstellar objects that are exposed to harsh galactic environments should resemble the surfaces of cold classical KBOs. Somewhat surprisingly, published measurements of the colour of 1I/'Oumuamua are more broadly consistent with the material in the inner Solar System and the object lacked ultra-red material.

2.3.3. Shape

For the majority of Solar System objects, photometric light curves provide the only information available regarding the shape of the object. Sometimes the shape models inferred from light curves can be verified and/or updated with radar measurements. Notable examples include the 'dog-bone' shaped asteroid (216) Kleopatra [93] and 1998 KY_{26} [94]. In special cases, in-situ space-based measurements reveal detailed geometry and terrain features. Therefore, much effort has gone into interpreting the shape of an object from photometric light curves alone.

The composite light curve of 1I/'Oumuamua displays several salient features [66,77]. The first is that the brightness varied by a factor of about ∼12–note that the *y*-axis in most published depictions of the lightcurve figure is in the scale of visual magnitudes, which is a logarithmic scale. At the time of the detection of 1I/'Oumuamua, no object in the Solar System had displayed such extreme amplitude brightness variations. It is worth noting that since the discovery of 1I/'Oumuamua, the NEO 2016 AK_{193} exhibited brightness variations of ∼2.5−−3 magnitudes during its discovery apparition and in subsequent followup observations [95]. Measurements of 2021 NY_1 and 2022 AB were reported by [96] indicating aspect ratios of $\geq$ 3.6 and $\geq$ 1.6 respectively.

The effects of both the orbital configuration and the geometry of an object can lead to amplitude variations, which can be difficult to disentangle. The phase angle, or the angle between the object sun and observer, can increase the amplitude of the light curve variations. Lightcurve variations are intrinsically driven by two features: an (i) elongated shape of the body and/or a (ii) nonuniform reflectance (or abledo) across the surface of the object. In the case of 1I/'Oumuamua, the aspect ratio implied by the lightcurve is 6:1 when correcting for the phase of the object throughout its trajectory. However, literature estimated of the aspect ratio varied from 5:3:1 [74], 6:1 by [68,97] to 10:1 [71]. It was unclear whether the elongation corresponded to a prolate or oblate ellipsodal geometry at the time of the discovery. A rigorous and exhaustive fit to the light curve using ∼1 GPU-year of computational time was performed by [98] demonstrating that the oblate or 'thin-disk' geometry with a 6:1 aspect ratio was favoured with a 91% likelihood. In retrospect, this geometry is intuitive because only an oblate geometry would produce deep minima during each circulation. The extreme shape was suggested to be the result of continuous bombardment and abrasion by interstellar dust particles [99–101], a violent collision [102], a tidal disruption of a larger object that came too close to a giant planet [103] or its parent star [104] before it was ejected to interstellar space, or a fractal aggregate structure [105]. It should be noted that a geometry of an ultra-thin minor axis was shown to produce a low (∼ 1%) probability of generating the observed large amplitude [106].

To recreate these types of variations from only albedo features, the object would need to have one hemisphere darkened with respect to the other. Space weathering and processing in the ISM would have been approximately isotropic. Therefore, this interpretation has been more or less disregarded. However, alternative reflection models such as Lambertian or specular reflection and single scattering diffusive and backscatter could plausibly reproduce the observed brightness variations with a less extreme aspect ratio [107].

The second salient feature is that there is an approximately constant periodicity of ∼8 h. If the object was elongated and rotating then each cycle would correspond to complete circulations as the objected reflected sunlight from the maximum and minimum cross-sectional areas. While the amplitude variations maintain constant periodicity, each individual cycle exhibits significant asymmetries. This was highlighted in [73], who showed phase-folded photometric data obtained with Gemini North telescope on 2017 October 27 and 28. The folded data show ∼10% differences at each circulation. This was interpreted as the object existing in an excited or tumbling rotational state [73,77,78]

2.4. Nongravitational acceleration

Despite the lack of visible dust coma or detected outgassing species, [108] reported a 30-σ significant detection of nongravitational acceleration in 1I/'Oumuamua's trajectory. This acceleration was based on astrometric fitting over a 2.5 month arc of the orbit.

The only significant component of the nongravitational acceleration of 1I/'Oumuamua was the radial component A_1, where $A_1 \sim 2.5 \times 10^{-4}\,\mathrm{cm\,s^{-2}}$ at $r \sim 1.4$ au to a 30-σ significance. The best fitting $g(r_H)$ functions for the nongravitational acceleration were those that depended inversely on the distance with exponents ranging from r_H^{-1} to r_H^{-2}. It is important to note that the exponent could not be constrained any better than being somewhere in the -1 to -2 range. The magnitudes of the best fitting nongravitational acceleration components in the transverse and normal directions were consistent with zero. In [108] it was concluded that the most likely cause of the nongravitational acceleration was outgassing. While some asteroids exhibit nongravitational accelerations caused by the Yarkovsky effect and radiation pressure (see Sections 2.6.1 and 2.6.2), the magnitude of the acceleration was too large to be explained by these effects. The nongravitational

acceleration combined with the lack of visible coma led to a wide array of hypotheses regarding the provenance of the object which we review in the following subsection.

2.5. The provenance of 1I/'Oumuamua

2.5.1. Radiation pressure-driven fractal aggregate or membrane

The two main causes of nongravitational accelerations seen on asteroids are the Yarkovsky effect [109] and solar radiation pressure [110]. The Yarkovsky effect results from anisotropic reradiation of thermal photons and typically manifests in the transverse $\hat{\mathbf{t}}$ direction. Solar radiation pressure is only detected in the radial $\hat{\mathbf{r}}$ direction and is weaker than outgassing effects but stronger than Yarkovsky effects for typical size and compositions of asteroids. Therefore it has only been measured on a handful of small asteroids [111–117]. For a more detailed discussion, we refer the reader to Sections 2.6.1 and 2.6.2.

Radiation pressure is therefore a natural explanation for the source of the acceleration of 1I/'Oumuamua, which was only significant in the radial direction. However, this was originally considered and dismissed by [108] because it would imply an extremely low bulk density or minor axis thickness. Given the lack of detectable dust coma, the hypothesis of radiation pressure induced acceleration was reconsidered by several authors. The theories that were published invoking radiation pressure can be categorised by those invoking (i) a naturally produced, ultra-low density aggregate [105,118,119] or (ii) a membrane-like structure of a very thin material (less than a mm thick) of an unknown natural or artificial origin, similar to a lightsail [120].

Regarding the former, a fractal aggregate with a density of $\sim 10^{-5}$ g cm^{-3} (about 100 times less than air) could provide the surface-to-mass ratio required to account for the observed acceleration of 1I/'Oumuamua [105,118]. A fractal structure could also help explain its unusual shape. However, the lowest density solid known (10 times less dense than air) is graphene aerogel and is synthetically produced. Therefore, it is unclear how such an ultra-porous structure could be naturally produced.

Fractal aggregates are found in many forms of nature and are thought to arise naturally because their formation processes involve an element of stochasticity. In a protostellar disk, the relative motions of neighbouring dust particles are small and therefore collisions are gentle. These conditions may be amenable to diffusion-limited aggregation [121]. Numerical simulations investigating planetesimal growth via dust collisions in a protoplanetary disk show that beyond icelines, if the tiny dust particles are covered with ice and are about 0.1 μm in size, the aggregates that form will have increasingly smaller densities as they grow [122,123]. This occurs because in the early phases when the particles are small and strongly coupled to the gas, the relative velocities of the colliding aggregates is low. Therefore, the collisions are not energetic enough to restructure the aggregates. This leads to a rapid increase of porosity as the aggregate grows. As the aggregates become larger, collisional compression occurs. However, this compression is inefficient and the porosity of the growing aggregate continues to increase. This increase occurs because most of the colliding energy is spent compressing the new voids that are created when two aggregates collide and stick to each other, rather than compressing the voids that were already present in the colliding aggregates (see review by [124]). What these studies show is that at ~ 100 m, about the size of 1I'/Oumuamua, the planetesimals can obtain ultra-low densities that are comparable to what would be required for 1I/'Oumuamua to be 'pushed' by radiation pressure [123]. It was therefore suggested that 1I/'Oumuamua could be one of these intermediate products of the planet formation process [105].

If this was its origin, it would be extraordinarily exciting because very little is known about these intermediate/early products of planet formation. Studying these objects could help set unprecedented constraints on planet formation models. In particular, the intermediate stage of planet formation, in which cm-sized particles grow into km-sized planetesimals, is not well understood because that process should theoretically be very inefficient. Several mechanisms have been proposed to help overcome this 'meter-sized barrier' and one of them is the presence of very high porosity planetesimals. The high porosity could favour the growth process because the larger cross section [122] would allow a longer lifetime against the effect of radial drift in the inner regions of the protoplanetary disk. This would both facilitate growth [123] and make the colliding aggregates less susceptible to fragmentation and bouncing.

There are other origins that have been proposed for an ultra-low density 1I/'Oumuamua. Coma aggregates collected from 67P/Churyumov-Gerasimenko with the ESA Rosetta mission had low densities < 1 kg m^{-3} [125] and fractal structure [126]. It was therefore hypothesised that 1I/'Oumuamua was a similar but larger-scale fractal aggregate formed in the coma of an active comet, that then escaped [119]. Another suggestion is that it was an ultra-porous desicated fragment that resulted from the disintegration of an 'ordinary' and larger interstellar comet as it passed near perihelion [118].

Regarding the survival of such an ultra-porous structure to the hazards of interstellar travel, somewhat counter-intuitively, [127] demonstrated that it could be stable to tidal disruption. Furthermore, they argued

that the interaction of such an ultra-low density aggregate with the solar radiation could explain the changes observed in the rotational period of 1I/'Oumuamua. It remains to be studied if this fractal structure could survive the ejection from its parent system and the passage near the Sun.

2.5.2. Tidally-disrupted planetesimal or planet fragment

The extreme aspect ratio of 1I/'Oumuamua remains somewhat of a mystery. In another line of reasoning, several authors considered that its extreme shape was primordial and caused by tidal forces. Tidal forces can have significant effects on small bodies like comets and asteroids. These manifest as body deformation in the mildest cases and catastrophic disruption in the most extreme cases. A notable example is the tidal disruption of the comet Shoemaker-Levy 9 when it passed close to Jupiter [128–131]. Chains of craters on the surfaces of Callisto and Ganymede may have been caused by catastrophic disruption of objects that subsequently impacted these surfaces [132]. Double craters that are seen on Solar System bodies [133–137] may have been caused by objects that underwent satellite formation from tidal disruption [138].

If 1I/'Oumuamua was ejected from its host system following a close encounter with a giant planet or its host star, it is possible that it too was subject to tidal forces that produced an elongated fragment. The dynamical simulations in [103,139,140] show that ∼1% of planetesimals pass within the tidal disruption radius of a gas giant on their pathway to ejection. If 1I/'Oumuamua was ejected from its host system following such a close encounter with a giant planet, it is possible that it too was subject to tidal forces, producing an elongated fragment [103,139,140]. Furthermore, these studies argued that these fragments might have a characteristic size of ∼ 100 m, similar to 1I/'Oumuamua's size, as opposed to a wider size distribution. Alternately, [104] proposed that 1I/'Oumuamua is a fragment that resulted from the tidal disruption of a planet, or a small body, that came too close to its parent star and that was later ejected to interstellar space. Based on detailed numerical simulations for a range of impact parameter and material properties, they suggested this process could produce a prolate object with the observed aspect ratio.

However, [98] demonstrated that the oblate shape was by far the most likely geometry of the object, which casts into doubt both tidal fragment hypothesis as the source of the extreme geometry. Moreover, [141] demonstrated that the lightcurve of 1I/'Oumuamua was consistent with no tidal deformation during its observed passage through the inner Solar System.

2.5.3. Sublimating icy comet

In [108], it was argued that the most natural explanation for the nongravitational acceleration was cometary outgassing. However, [142] compared 1I/'Oumuamua to comets for which the rotational periods of the nuclei had been measured and argued that the magnitude of the nongravitational acceleration should have caused a measurable change in the nuclear spin period. Using an outgassing model, [143] argued that a rapidly mobilising outflow that tracked the point of maximal solar irradiance would not result in significant spin-up of the object. However, this model is highly idealised and in reality cometary nuclei do experience secular spin-up that can lead to disintegration [144–156]. In [127], it was reported that in the high-cadence data of 2017 October, 1I/'Oumuamua experienced a slight spin-down in its rotational period that could be attributed to the YORP effect on a fractal body with low ultra-low density.

A further issue with the outgassing hypothesis is that 1I/'Oumuamua did not receive sufficient energy in the form of solar irradiation to power typical outgassing of H_2O or CO_2 (see Sections 1.4 and 1.5) [157]. The sublimation rate per unit surface area can be calculated as an equilibrium solution (as described in Section 4.1 of [66]) to the equation

$$\left(\underbrace{\frac{(1-p)L_\odot}{4\pi r_H^2}}_{\text{Solarenergy}}\right) k_R = \underbrace{\varepsilon\sigma T_S^4}_{\text{Re-radiated}} + \underbrace{Hf_s(T_S)}_{\text{Sublimation}} + \underbrace{C(T_S)}_{\text{Interior}}. \tag{4}$$

In Equation (4), p is the albedo, r_H the heliocentric distance, $L_\odot$ is the Solar luminosity, ε is the surface thermal emissivity, σ is the Stefan–Boltzmann constant, T_S (K) is the temperature at the surface, H is the latent heat of sublimation, $f_s(T)$ is the sublimation rate and k_R is the degree of collimation of the outflow described in Equation (2). The LHS of Equation (4) is the total energy received from solar radiation, and the RHS indicates the total energy required to produce the outflow. On the RHS, $\varepsilon\sigma T_S^4$ is the energy reradiated from the surface of the comet, $Hf_s(T_S)$ is the energy deposited in the form of the latent heat of sublimation to convert the ice into a gas, and $C(T_S)$ represents heat conduction into the interior. The last term is negligible in most cases.

Equation (2) can be solved using both the nongravitational acceleration magnitude and fiducial size of 1I/'Oumuamua. This produces a required sublimation rate of $\dot{M} = 24\,\mathrm{kg\,s^{-1}}$ needed to provide the acceleration [66]. From Equation (4), H_2O and CO_2 are insufficient to provide this sublimation for 1I/'Oumuamua due to the relatively high latent of these species. Since H_2O and

CO_2 are the most common volatiles seen in Solar System comets (see Section 1.5), if 1I/'Oumuamua was outgassing it is unlike most icy objects we have seen in the Solar System. [158] demonstrated that when considering these bulk energetics, only hypervolatiles such as molecular hydrogen H_2, molecular nitrogen N_2, CO or more exotic species such as Xenon, Neon, Krypton or Argon could have been feasible accelerants. The noble gases, however, exhibit relatively low cosmic abundance and are therefore a priori not likely to be bulk constituents of 1I/'Oumuamua.

The subsurface layers of 1I/'Oumuamua are required to reach sufficient temperatures for the outgassing volatiles to sublimate to power the acceleration. In [68], it was first estimated that the thermal skin depth of 1I/'Oumuamua was ~0.5 m via an order of magnitude calculation to argue that the internal temperature could remain at ~10 K throughout the trajectory. In [72], a more detailed numerical thermal model was presented that demonstrated H_2O was stable to depths of $\gtrsim$30 cm (see figure 4 in [72]). The thermal modelling of the interior requires numerical solutions to the heat conduction equation,

$$\frac{\mathrm{d}T}{\mathrm{d}t} = \frac{\kappa}{\rho_{Bulk} c_P} \frac{1}{z} \frac{\partial}{\partial z} \left(z \frac{\partial T}{\partial z} \right). \tag{5}$$

In Equation (5), T is the temperature, κ is the thermal conductivity, c_P is the specific heat capacity and z is the depth. The thermal properties of 1I/'Oumuamua are entirely unconstrained, but typical cometary properties are $\rho_{Bulk} = 0.5\,\mathrm{g\,cm^{-3}}$ [159], $c_P = 2000\,\mathrm{J\,kg^{-1}}$ and $\kappa = 10^{-2} - 10^{-1}\,\mathrm{W\,K^{-1}\,m^{-1}}$ [160]. We show the results of this thermal modelling for 1I/'Oumuamua in Figure 4, with the sublimation temperatures of H_2O, CO_2 and CO in the top panels. The remaining volatile species have been investigated further but, because of theoretical and/or observational arguments, none are thought to be the prime constituent of 1I/'Oumuamua.

In [158], the hypothesis that 1I/'Oumuamua was composed of solid H_2 was explored. H_2 has a sublimation temperature of ~6 K and this scenario suggested that

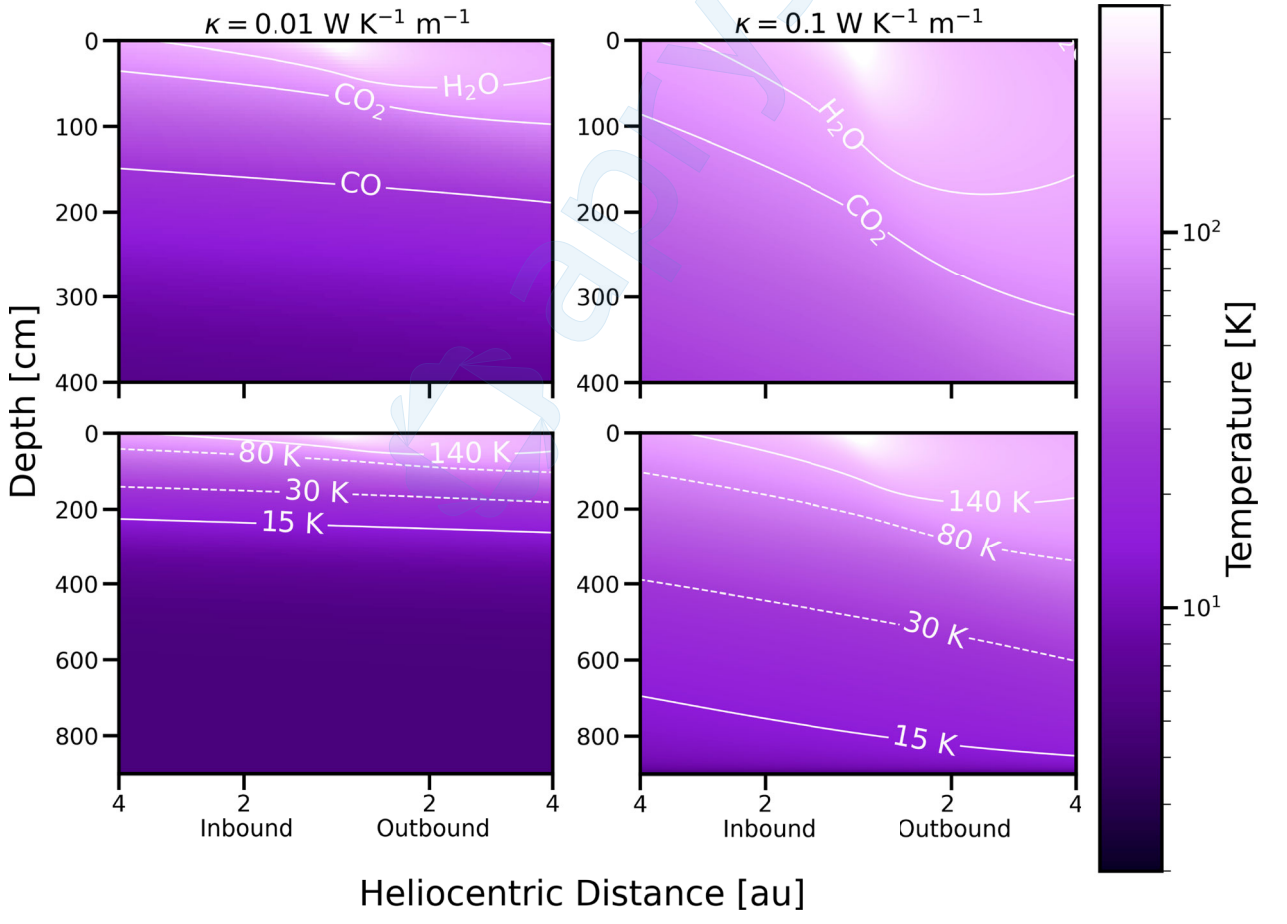

Figure 4. Numerical solutions of the radial heat equation (Equation 5) for 1I/'Oumuamua spanning the inbound and outbound trajectories interior to 4 au. We adopt a bulk density $\rho_{Bulk} = 0.5\,\mathrm{g\,cm^{-3}}$, specific heat capacity of $c_P = 2000\,\mathrm{J\,kg^{-1}\,K}$ and thermal conductivity $\kappa = 10^{-2}\,\mathrm{W\,K^{-1}\,m}$ (left panels) and $\kappa = 10^{-1}\,\mathrm{W\,K^{-1}\,m}$ (right panels). Contours on the left panels indicate sublimation fronts of CO (28 K), CO_2 (86 K) and H_2O (144 K) [169]. Contours on the right panels indicate where H_2 outgassing is expected during the annealing of amorphous H_2O ice for temperatures of ~15–140 K. Adapted from [170].

1I/'Oumuamua originated in a failed prestellar core of a giant molecular [161]. The continuous ablation of H_2 from the surface via cosmic ray exposure and solar photons would naturally produce the elongated shape. Other authors argued that the cosmic radiation would have destroyed a macroscopic H_2 body before it reached the Solar System [162,163], although [164] showed that km-scale progenitors could survive for timescales $\leq$ 100 Myr. However, any theory must account for not only the existence of 1I/'Oumuamua, but also for the progenitor galactic population of similar-sized objects. This population is inferred to exist based on 1I/'Oumuamua's detection frequency and is estimated to contain $\sim 10^{26}$ objects (see discussion in Section 4.1). The primary caveat with the solid H_2 scenario is that the frigid temperature requirements for the prestellar cores would be extremely challenging to achieve ubiquitously throughout star forming regions to account for the progenitor population of interstellar objects.

It was subsequently hypothesised that 1I/'Oumuamua was composed of solid N_2 instead, implying that it was a remnant from an impactor event on an exo-Pluto analogue that generated significant fragments of solid nitrogen [165,166]. Given that such bodies are large enough to differentiate volatiles, this theory may also explain the lack of dust coma seen in the object. However, this would require a very high efficiency of ejection of nitrogen-rich material from planetary systems if stellar populations were producing such objects uniformly exacerbated by the fact that high velocity impactors do not generically produce fragments with sufficient kinetic energy to escape from the host body [167]. However, some of these issues would be alleviated if only M stars produced 1I/'Oumuamua like interstellar objects and if the typical impacts were at indirect impact angles [168]. If this theory proves correct, then it is possible that the discovery of 1I/'Oumuamua was an outlier event, and we can expect few or no similar discoveries in the future [167].

In [81], it was investigated whether CO outgassing could produce the nongravitational acceleration, despite the nondetection with *Spitzer*. While theoretically viable, this explanation requires a highly fine-tuned sporadic outgassing throughout the trajectory.

In [170], it was demonstrated that the crystallisation of amorphous water ice would provide sufficient radiolytically-produced and entrapped H_2 to account for the observed nongravitational acceleration. Energetic processing of an H_2O-rich icy body irradiated by galactic cosmic rays would produce entrapped H_2, a process that has been demonstrated in laboratory experiments [171–177]. This crystallisation would occur in the absence of sublimation of the overall ice matrix, thereby explaining the lack of dust coma observed.

This explanation requires the subsurface of 1I/'Oumuamua to reach sufficient temperatures to crystallise ice via annealing of the amorphous water matrix. Moreover, the required temperatures between 15 and 140 K [172,175,178] must be reached at sufficient depths within the interior to produce sufficient H_2 to power the acceleration, given a laboratory measured $\sim$20−−35% yield of entrapped H_2 [172]. More realistic H_2/H_2O yields of tens of percent are predicted for the subsurface metres of a porous cometary composition exposed to cosmic rays [179], which can penetrate to depths of tens of metres [180].

Solutions to the thermal depths presented in [170] are shown in Figure 4. Indeed, the subsurface metres reach sufficient temperatures to crystallise amorphous ice without producing significant H_2O sublimation. This explanation would therefore partially explain the lack of observed dust (Table 1). Without the bulk ice matrix sublimating, the release of entrapped H_2 within a few metres of the subsurface would not release dust trapped within the ice matrix. The lack of surface dust may be due to interactions with ambient gas in the interstellar medium which preferentially remove small dust grains from the surface of long-period comets and interstellar comets [181].

2.6. 1I/'Oumuamua in the context of solar system asteroids

2.6.1. Active asteroids

Small bodies throughout the Solar System have classically been categorised based on their volatile-driven activity. Comets were defined as icy objects that produced dusty comae and presumably spent little or no time in the inner Solar System. Meanwhile, asteroids lacked volatiles due to their closer proximity to the Sun which subjects them to prolonged and intense irradiation. However, recent advances have shown that this simple classification is not entirely accurate. Specifically, a subset of asteroids appear active and either have detectable dust activity or nongravitational accelerations potentially caused by outgassing [182–184]. Within this context, the active asteroids are directly relevant to 1I/'Oumuamua which displayed a hybrid of cometary and asteroidal properties.

The Main Belt Comets (MBCs) reside in the asteroid belt and display low levels of cometary activity [185]. The first MBC to be discovered was Comet 133P/(7968) Elst-Pizarro [186–189]. Several other MBCs have since been identified, and occurrence rates of $< 1/500$ and $\sim 1/300$ have been inferred from surveys [190–193].

The cause of dust activity in these active asteroids is not completely clear. As discussed previously, outgassing induces nongravitational accelerations [49,50]

which have been detected on some active asteroids with related dust activity [194]. However, other effects caused from impacts [195] and rotation [196] can produce dust activity in the absence of outgassing.

Intriguing cases of active asteroids that do not exhibit obvious outgassing are (3200) Phaethon and (101,955) Bennu, the target of the OSIRIS-REx mission. (3200) Phaethon was first identified to be active because of its association with the Geminid meteoroid stream [197,198]. It produces a small dust tail around perihelia with optically observed micron-sized dust production rates of $\sim$3 kg s^{-1} [199–202]. However, this level of activity was incompatible with the flux from the meteoroid stream. Therefore other effects such as thermally induced stresses [199], sublimation of minerologically bound sodium [203], rotation [204,205] and geometry [206,207] have been used to explain the activity. (101,955) Bennu was identified as active only when particle ejection events were measured by the OSIRIS-REx spacecraft [208,209]. The measured mass flux was $\dot{M}_{\rm Dust} \sim 10^{-4}$ g s^{-1} [210]. However, the source of the activity of (101,955) Bennu remains unsolved [211–213].

2.6.2. Dark comets (inactive asteroids experiencing nongravitational accelerations)

At the time of 1I/'Oumuamua's discovery, there had been no asteroidal objects discovered that exhibited nongravitational accelerations with no dust activity. As discussed previously, nongravitational accelerations have been measured on inactive asteroids due to the Yarkovsky effect and radiation pressure. However, the magnitudes of these accelerations are typically much lower than those discovered on 1I/'Oumuamua. Since the detection of 1I/'Oumuamua, a new population of inactive asteroids has been discovered that exhibits stronger nongravitational accelerations and similarly lacks dust comae. We refer to these as dark comets.

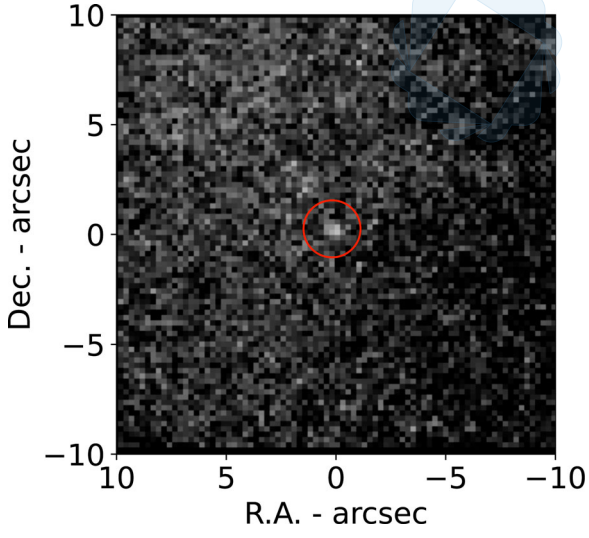

Figure 5. The dark comet 1998 KY$_{26}$ which exhibits no dust coma and a significant nongravitational acceleration. The image was taken with the VLT and incorporates $\sim$1 h of temporal coverage in 2020 December. The $\sim$30 m object is faint and indicated with a red circle. Reproduced from [214].

Namely, [214–216] reported statistically significant detections of non-radial nongravitational accelerations in a sample of photometrically inactive NEOs. The objects with nongravitational accelerations inferred from astrometric data are (523,599) 2003 RM, 1998 KY$_{26}$, 2005 VL$_1$, 2016 NJ$_{33}$, 2010 VL$_{65}$, 2006 RH$_{120}$ and 2010 RF$_{12}$. In Figure 5, we show a stack of VLT images of one of these objects, 1998 KY$_{26}$, taken during 2020 December. This image contains a stack of exposures resulting in a composite image with a total of 3600 s exposure. The object quite clearly lacks a dust tail and, because of this and the nongravitational acceleration, is reminiscent of 1I/'Oumuamua. The image corresponds to an upper limit of dust production of $\dot{M}_{\rm Dust} < 0.2$ g s^{-1}.

All of the dark comet nongravitational accelerations are inconsistent with being caused by radiation pressure or Yarkovsky effect, demonstrated in Figure 6. The best fitting nongravitational acceleration parameters and their significance are shown in Table 2. The significant A_2 and A_3 are inconsistent in magnitude with radiation pressure and the Yarkovsky effect. Therefore [214,216] argued that these accelerations were caused by outgassing with no (or low levels of) accompanying dust comae.

These dark comets may be Solar System analogues of 1I/'Oumuamua, in that they have measured nongravitational accelerations and no (or low levels of) dust comae. The lack of dust has been attributed to low levels of outgassing and presumably a lack of surface dust. Although 1I/'Oumuamua is now long gone, investigating these dark comets may reveal similar physical processes that can produce outgassing and nongravitational accelerations without significant dust production. The JAXA Hayabusa2 extended mission will rendezvous with 1998 KY$_{26}$ [217]. The instrument suite onboard Hayabusa2 can measure volatile and dust production [218–229]. Therefore, the nature of the nongravitational acceleration of these possible Solar System analogues of 1I/'Oumuamua should be definitively identified in the near-term future.

3. 2I/Borisov

3.1. Discovery

The comet C/2019 Q4 (Borisov) was discovered on 2019 August 30 when it was close to the sun with an angular separation of just 38°. This object was discovered by

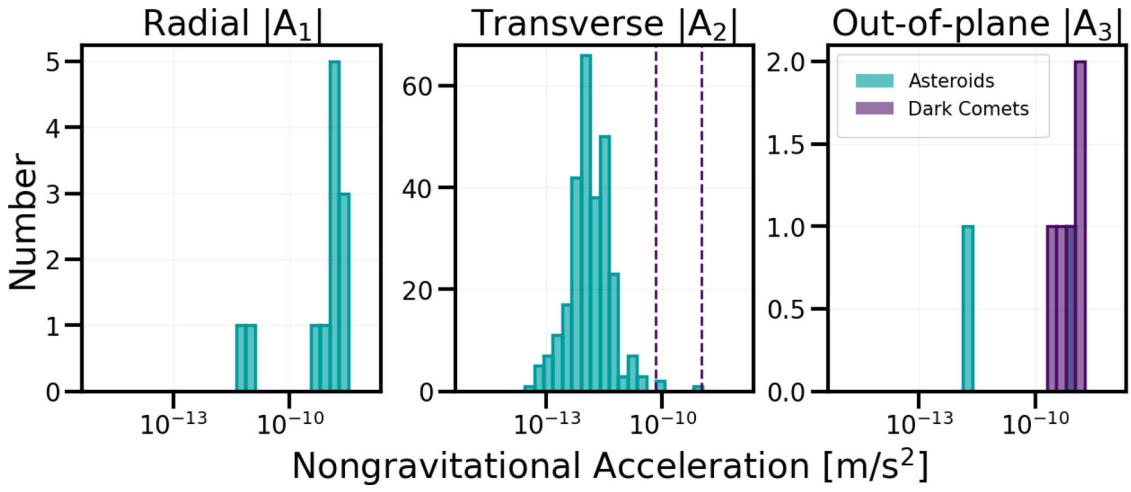

Figure 6. Nongravitational accelerations measured in asteroids (teal) and dark comets (purple), similar to Figure 1. Measured radial nongravitational acceleration A_1 are due to solar radiation pressure (left) and transverse acceleration A_2 are due to the Yarkovsky effect (middle). The out-of-plane nongravitational acceleration A_3 measured in the objects (right) are presumably due to polar outgassing events. Dark comet candidates with anomalous A_2 values, 2003 RM and 2006 RH_{120}, are shown in purple dashed lines in the middle panel.

Gennadiy Borisov, an amateur astronomer using a 0.65-m telescope. It is worth noting that the object was not discovered by the all sky surveys searching for transient events, which intentionally do not observe near the Sun.

Like 1I/'Oumuamua, the trajectory of the comet is definitively of interstellar origin, with an escape velocity, $v_\infty = 32.304 \pm 0.001$ km/s, semimajor axis of $a = -0.850$ au, eccentricity of $e = 3.363$, inclination $i = 44.0°$ and perihelion of $q = 2.009$ au. Because of the definitive interstellar trajectory, it was renamed to 2I/Borisov. Unlike 1I/'Oumuamua, the object was discovered ~3 months prior to perihelia which left ample time for characterisation with subsequent telescopic observations. In Figure 7, we show an image of 2I/Borisov taken with the *Hubble Space Telescope* [230].

3.2. Nucleus properties

3.2.1. Size

The images of 2I/Borisov obtained with HST [231] provided empirical evidence for a nuclear radius of 0.2–0.5 km. This was supported by upper limits from ground-based infrared imaging [232]. The upper limit was derived from modelling the brightness profile of the coma, and the lower limit was derived from the measured nongravitational acceleration assuming a bulk density representative of comets to prevent catastrophic disruption due to outgassing forces [230]. This nuclear size is more in line with Solar System comets and provides a stark contrast to the very small size inferred for 1I/'Oumuamua.

Table 2. Dark comets with nongravitational accelerations and no observed dust production.

Object	a [au]	e	i [°]	q [au]	H [mag]	r_n [m]	P_{Rot} [h]	A_1 [10^{-10} au d^{-2}] Signif.[σ]	A_2 [10^{-10} au d^{-2}] Signif.[σ]	A_3 [10^{-10} au d^{-2}] Signif.[σ]
2003 RM	2.92	0.60	10.86	1.17	19.80	230		-1.045 ± 1.217 <1	0.0215 ± 0.0004 56	0.0156 ± 0.0543 <1
1998 KY_{26}	1.23	0.20	1.48	0.98	25.60	15	0.178	1.73 ± 0.91 2	-0.00126 ± 0.00061 2	0.320 ± 0.115 3
2005 VL_1	0.89	0.23	0.25	0.69	26.45	11		-6.66 ± 8.02 <1	-0.00711 ± 0.00592 1	-0.240 ± 0.041 6
2006 RH_{120}	1.00	0.04	0.31	0.96	29.50	2–7	0.046	1.38 ± 0.08 18	-0.507 ± 0.0637 8	-0.130 ± 0.032 4
2010 VL_{65}	1.07	0.14	4.41	0.91	29.22	3		6.57 ± 13.0 <1	-0.00146 ± 0.00534 <1	-0.913 ± 0.130 7
2010 RF_{12}	1.06	0.19	0.88	0.86	28.42	4		0.488 ± 0.597 <1	-0.00136 ± 0.00286 <1	-0.168 ± 0.021 8
2016 NJ_{33}	1.31	0.21	6.64	1.04	25.49	16	0.41–1.99	9.28 ± 2.96 3	0.00566 ± 0.00193 3	0.848 ± 0.163 5

Notes: Best-fit nongravitational acceleration parameters for each object are shown with 1–σ uncertainties. P_{Rot} is the rotational period and H is the reported absolute magnitude. Reproduced from [214].

Figure 7. The second interstellar comet discovered, 2I/Borisov. The image was taken with HST on 2019 October 12 [230]. 2I/Borisov displays a clear cometary tail. r_H corresponds to the heliocentric distance of the object when the image was obtained. Reproduced from [230].

3.2.2. Colours

2I/Borisov displayed a distinct dust and gas coma and was unmistakably a comet [231–235]. The measured colours of 2I/Borisov, unlike for 1I/'Oumuamua, were representative of the colour of the ejected dust which dominate the images. The dust ejected from 2I/Borisov was reddened with respect to that of the Sun, similar to 1I/'Oumuamua. Early spectral observations with the 10.4 m Gran Telescopio Canarias (GTC) revealed a visible spectrum with a spectral slope that is roughly in the middle of the range of visible spectral slopes observed for cometary nuclei in the Solar System [236]. The dust in the cometary tail was measured to have a slightly reddish colour of $g' - r' = 0.63 \pm 0.03$ [231–233], later measured as $g' - r' = 0.68 \pm 0.04$ and $r' - i' = 0.23 \pm 0.03$ [234].

3.2.3. Nongravitational acceleration

With 10 months of astrometric positional data, it was evident that 2I/Borisov exhibited nongravitational acceleration. Similar to 1I/'Oumuamua, the dominant component of the nongravitational acceleration was in the radial direction, with $A_1 = 7.1 \pm 0.8 \times 10^8$ au d^{-2}, $A_2 = -1.4 \pm 0.3 \times 10^8$ au d^{-2} and $A_3 = 0.1 \pm 1.5 \times 10^8$ au d^{-2}. These were consistent with being recoil effects from measured production rates [234,237,238]. In Figure 8, we show the nongravitational accelerations measured in comets, asteroids, dark comets, 1I/'Oumuamua and 2I/Borisov. We limit to only objects that have sizes measured.

3.3. Coma properties

3.3.1. Dust properties

VLT and ALMA data of 2I/Borisov was reported by [239] showing that that the dust in the coma contained a contribution from pebbles with sizes $\gtrsim 1$ mm. Dust production rates of $Q(\text{dust}) = 35\,\text{kg s}^{-1}$ (2019 November) and $Q(\text{dust}) = 30\,\text{kg s}^{-1}$ (2019 December) were reported by [240] using observations with the Telescopio Nazionale Galileo. The contributing dust grains were consistent with sizes mostly larger than 100 μm [241].

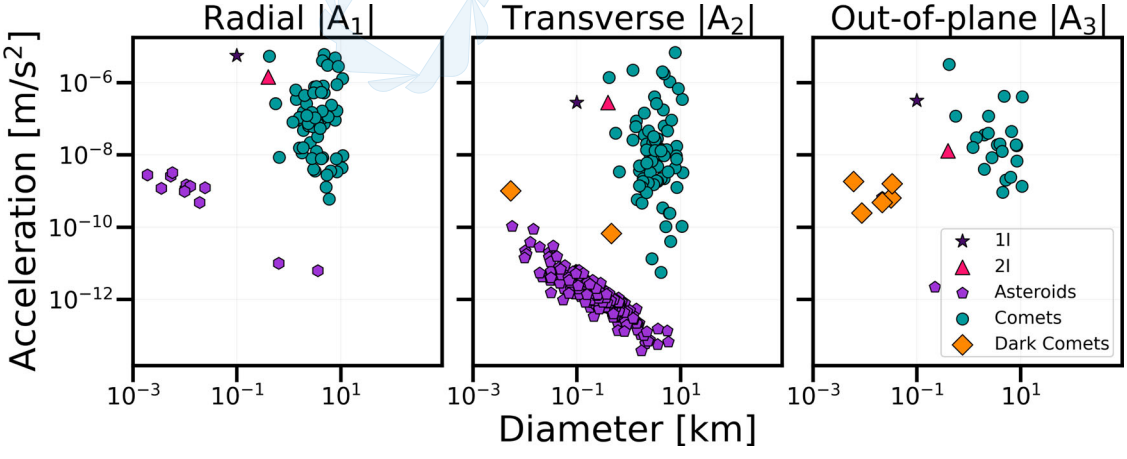

Figure 8. Measured nongravitational accelerations of a variety of small bodies. The three panels show measured components of nongravitational accelerations in the radial A_1 direction (left), transverse A_2 direction (middle) and out-of-plane A_3 direction (right). In each panel, measured nongravitational accelerations of comets (teal circles) asteroids (purple hexagons), dark comets (orange diamonds), 1I/'Oumuamua (dark purple star) and 2I/Borisov (magenta triangle) are shown. Only comets with measured nuclear diameters are shown – many more comets exist for which nongravitational accelerations have been measured (Figure 1). The size of the asteroids have been approximated using Equation (3).

The presence of submicron sized conglomerates of magnesium-ferrous particles was inferred from photometric observations for ∼2 months before periastron [242]. Polarimetric measurements of the object obtained by the ESO Very Large Telescope intriguingly showed that the dust in the outflow exhibited a high level of polarisation compared to levels seen in dust produced in typical Solar System comets [243]. This polarisation was further shown to be consistent with a high ∼80% fraction of rough fractal aggregates and ∼20% of agglomerated debris, interpreted as 2I/Borisov having a large percentage of small and porous *pristine* cosmic dust particles [244].

3.3.2. Volatile composition

The orbit and discovery of 2I/Borisov enabled several months of detailed compositional measurements to be obtained. While the object was definitively a comet unlike 1I/'Oumuamua, its composition was different than those typically seen in Solar System comets. These observations are summarised in Tables 3 and 4.

Initial measurements of the object showed that H_2O was active as early as 6 au and inbound [231,250,255]. Subsequent observations revealed carbon and nitrogen bearing species in the coma. Near-UV emission of CN from 2019 September 20 was presented by [250] presented, together with an upper limit on the abundance of C_2, based on observations with the 4.2-m William Herschel Telescope and the ISIS spectrograph on La Palma. Measurements of CN and C_2 production were also reported by [251] using the 2.3-m Bok telescope at Kitt Peak National Observatory in Arizona, the 6.5-m MMT telescope located at Mount Hopkins, and the Large Binocular Telescope at the DDT. Similar spectroscopic detections and upper limits were reported by [246] using data from the 4.2-m William Herschel and 2.5-m Isaac Newton telescopes on a range of dates from 2019 September 30 to 2019 October 13. Detections of C_2 and of CN were reported by [256] using data from the MDM observatory Hiltner 2.4-m telescope and the Ohio State Multi-Object Spectrograph from 2019 October 31 and November 4. Additional observations were presented by [253] using the Multi-Unit Spectroscopic Explorer (MUSE) at the 8.2-m UT4 of the ESO/Very Large Telescope (VLT) and the 0.6-m TRAPPIST North and South telescopes.

Production rates and upper limits of H_2O were measured throughout the trajectory. A production rate of $Q(H_2O) = 6.3 \pm 1.5 \times 10^{26}$ mol s^{-1} was derived by [247] based on observations with the ARCES instrument at Apache Point Observatory on 2019 October 11, while [254] reported observations taken with the 2-m Himalayan Chandra Telescope located at the Indian Astronomical Observatory, Hanle (HCT) and the Mount Abu Infrared Observatory (MIRO) from 2019 November 30 and December 22 that yielded production rate ratios of $Q(C2)/Q(CN) = 0.54 \pm 0.18$ and $Q(C2)/Q(CN) = 0.34 \pm 0.12$ before and after perihelion respectively. Critically, [245] presented observations of production rates both before and after perihelion with 6 epochs of observations with the Neil Gehrels Swift Observatory's Ultraviolet/Optical Telescope. These revealed that the H_2O production increased and decreased before and after perihelion, and they estimated an active fraction of ≥ 55% of the surface to account for the inferred production.

Table 3. The production rates of molecules CO, H_2O and OH measured in the comae of 2I/Borisov.

Date	r_H [au]	$Q(H_2O)10^{26}$ [mol s^{-1}]	$Q(CO)10^{26}$ [mol s^{-1}]	$Q(OH)10^{26}$ [mol s^{-1}]	Reference
9/27/19	2.56	<8.2			[245]
10/2/19	2.50			<0.2	[246]
10/11/19	2.38	6.3 ± 1.5			[247]
10/13/19	2.36			<0.2	[246]
11/1/19	2.17	7.0 ± 1.5			[245]
12/1/19	2.01	10.7 ± 1.2			[245]
12/3/19	2.01		3.3 ± 0.8		[239]
12/11/19	2.01		7.5 ± 2.3		[248]
12/15–16/19	2.02		4.4 ± 0.7		[249]
12/19–22/19	2.03	4.9 ± 0.9	6.4 ± 1.4		[248]
12/21/19	2.03	4.9 ± 0.9			[245]
12/30/19	2.07		10.7 ± 6.4		[248]
1/13/20	2.16	<5.6	8.7 ± 3.1		[248]
1/14/20	2.17	<6.2			[245]
2/17/20	2.54	<2.3			[245]

Notes: r_H is the Heliocentric distance at observation. Adapted from [59].

Table 4. The production rates of molecules CN, C_2 and C_3 measured in the coma of 2I/Borisov.

Date	r_H [au]	Q(CN) 10^{24}[mol s^{-1}]	$Q(C_2)$ 10^{24}[mol s^{-1}]	$Q(C_3)$ 10^{24}[mol s^{-1}]	Reference
9/20/19	2.67	3.7 ± 0.4	<4		[250]
9/20/19	2.67	<5	<8		[251]
10/1/19	2.50	1.1 ± 2.0	<2.5		[251]
10/1/19	2.51	1.8 ± 0.1	<0.9	<0.3	[246]
10/2/19	2.50	1.9 ± 0.1	<0.6	<0.2	[246]
10/9/19	2.41	1.59 ± 0.09	<0.44		[251]
10/10/19	2.39	1.69 ± 0.04	<0.162		[251]
10/13/19	2.36	2.1 ± 0.1	<0.6	<0.3	[246]
10/18/19	2.31	1.9 ± 0.6			[246]
10/20/19	2.29	1.6 ± 0.5			[246]
10/26/19	2.23	1.9 ± 0.3			[251]
10/31/19	2.18	2.0 ± 0.2			[252]
11/4/19	2.15	2.4 ± 0.2	0.55 ± 0.04	0.03 ± 0.01	[252]
11/10/19	2.12	1.9 ± 0.5			[253]
11/14/19	2.09	1.8 ± 0.2	1.1		[253]
11/17/19	2.08	1.9 ± 0.5			[253]
11/25/19	2.04	1.6 ± 0.5			[253]
11/26/19	2.04	1.8 ± 0.2			[253]
11/26/19	2.04	1.5 ± 0.5	1.1		[253]
11/30/19	2.01	3.36 ± 0.25	1.82 ± 0.6	0.197 ± 0.052	[254]
12/22/19	2.03	6.68 ± 0.27	2.3 ± 0.82	0.714 ± 0.074	[254]

Notes: r_H is the Heliocentric distance at observation. Adapted from [59].

While these previously discussed observations were in line with compositions typically seen in Solar System comets, post perihelia observations demonstrated that the object was enriched in the hypervolatile CO [248,249]. Atacama Large Millimeter/submillimeter Array (ALMA) images were obtained on 2019 December 15 and 16, and revealed the presence of HCN and CO at high abundances relative to H_2O [249]. Similarly, [248] reported observations with the Cosmic Origins Spectrograph (COS) on the HST between 2019 December 11 and 2020 January 13, that revealed high CO production rates with respect to H_2O. Additional measurements of CO production by [239] found that the CO/H_2O mixing ratio changed drastically before and after perihelion.

A spectroscopic detection of atomic nickel vapour in the coma of 2I/Borisov at 2.322 au was reported by [257] using observations with X-shooter spectrograph at the ESO VLT on 2020 January 28, 30 and 31, when the object was at an equilibrium temperature ∼180 K. Atomic nickel vapour has been detected in sun-grazing comets such as the case of C/1965 S1 (Ikeya–Seki) [258,259]. However, this is typically observed at much warmer temperatures $>$ 700 K and attributed to the sublimation of metal enriched dust grains. These authors concluded that the nickel vapour was a photodissociation product of a short-lived nickel-containing molecule.

3.4. Breakup

2I/Borisov exhibited a stark brightening event [260] and subsequent breakup in the spring of 2020 [261–264]. HST observations of the breakup were presented in [261]. The splitting event can be seen in March, where the nucleus develops a two-lobed shape.

The evolution of the coma morphology of 2I/Borisov in the HST images was interpreted as evidence of seasonal effects [241]. Specifically, the changes in activity levels and breakup [261] could be explained by regions on the northern hemisphere of the nucleus being exposed to the sun for the first time (particularly, see figure 7 in [241]). Seasonal effects and nucleus disruption are typically seen in Solar System comets and have been attributed to cometary fading [265].

3.5. Borisov in the context of solar system comets

The composition of 2I/Borisov was anomalous compared to typical Solar System comets due to the high abundance of the hypervolatile CO. Contemporaneous observations sensitive to H_2O and CO revealed a production rate ratio of $Q(CO)/Q(H_2O) \geq 1$. It is important to note that this production rate ratio is calculated only when near-contemporaneous measurements of both species were obtained. As discussed previously in this review (see Sections 1.4 and 1.5), comets are typically composed primarily of H_2O, with average ratios of $Q(CO)/Q(H_2O) \sim$ 4% although with a wide range [57].

This was interpreted as 2I/Borisov having formed in a carbon rich environment. It was argued that 2I/Borisov likely formed in an M star system. In such a system, the relatively cooler temperatures would lead to a CO snowline closer to the star. This implies that the majority of the circumstellar solids lie outside the CO snowline [248]. Alternatively, [249] argued that 2I/Borisov formed close to or at the CO snowline and was possibly the remnant of an impacted exo-Kuiper belt object. This scenario is similar to that suggested for 1I/'Oumuamua in which it is a fragment of an exo-Pluto analogue [165,166,168]. All of these interpretations of the hypervolatile content indicate that the object formed exterior to the CO snowline in its original protoplanetary disk [266].

Interestingly, the abundance of remnant hypervolatiles can inform the timing of the ejection of 2I/Borisov from its host system. Even if it formed beyond the CO snowline and remained there, prolonged heating from stellar irradiation would have removed hypervolatiles at large stellocentric distances if exposed for 100 s of Myr. Therefore, [267] argued that the object must have been ejected within $<$20 Myr of the formation in its host system.

An intriguing comparison object is C/2016 R2 [58,268,269], a highly eccentric LPC that exhibits a CO to H_2O production rate ratio $\gtrsim$ 100 [58]. However, C/2016 R2 displayed a CO/H_2O ratio much higher than that of 2I/Borisov, and an unexpectedly high abundance of N_2 [268,270]. It has been suggested that C/2016 R2 is interstellar in origin because of its exotic composition [58]. In Figure 9, we show the compositions of 2I/Borisov and C/2016 R2. While not a direct analogue of 2I/Borisov, it is one of the few Solar System comets enriched in hypervolatiles and is certainly the most extreme case. Relevant to this discussion, the Solar System comets C/2009 P1 Garradd [271–274], C/2010 G2 Hill [275] and C/2006 W3 Christensen [60] have high abundances of CO relative to H_2O. C/1995 O1 (Hale-Bopp) had $Q(CO)/Q(H_2O) > 12$ measured at $r_H = 6$ au [276] and the Centaur 29P/SW1 exhibited $Q(CO)/Q(H_2O) = 10 \pm 1$, measured at $r_H \sim 6$ au [57,276]). However, at these further heliocentric distances, H_2O is typically not active. Therefore, the compositions measured at large distances are not necessarily representative of the volatile inventories.

4. Galactic population of interstellar objects

4.1. Number of interstellar objects

Prior to the detection of 1I/'Oumuamua, several studies had estimated the number density of interstellar

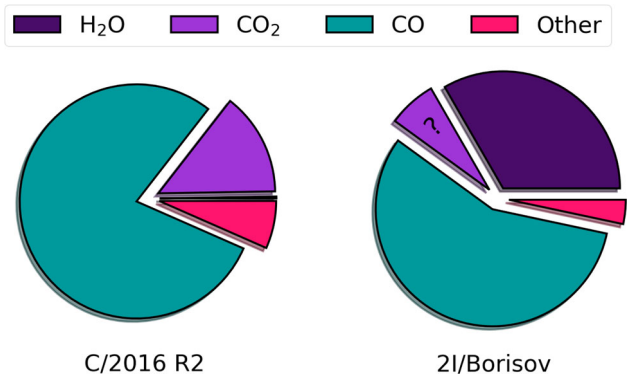

Figure 9. The compositions of 2I/Borisov and C/2016 R2, analogous to Figure 2. Note that there were no observations sensitive to CO_2 obtained for 2I/Borisov. Therefore, it is possible that the object had CO_2 in its outflow that was never measured as indicated with a question mark.

Table 5. Published estimates of the galactic space density of interstellar interlopers.

Reference	Density [$M_\odot$ pc^{-3}]	Density [au^{-3}]	Rate [yr^{-1}]
[280]	6×10^{-4}	$\lesssim 0.07$[a]	
[281]	2×10^{-5}	10^{-3} [a]	~ 0.6
[282]			< 0.01
[283]		$\sim 10^{-3}$ [a]	
[10]	3×10^{-6}	$3\text{–}4.5 \times 10^{-4}$	
[284]	$\sim 2 \times 10^{-7}$	3×10^{-5} [a]	
[285]		$< 1.4 \times 10^{-4}$	
[286]		$10^{-8}\text{–}10^{-5}$ [a]	
[68]		~ 0.1	
[277]		~ 0.1	
[278]		~ 0.2	
[279]		~ 0.2	
[287]	$\sim 3 \times 10^{-7}$ (singles)		
[287]	$\sim 1 \times 10^{-6}$ (binaries)		
[288]		$\sim 3 \times 10^{-3}$ (Oort cloud)	

[a] Objects greater than 1 km.

comets from non-detections. These are summarised in Table 5, dating back to 1976. Immediately before 1I/'Oumuamua's discovery, several studies provided detailed simulations of the expected galactic population of ejected comets and predicted the prospects for future detections with existing and forthcoming surveys.

The discovery of 1I/'Oumuamua implies that a much larger galactic population exists than was previously estimated. The occurrence rate of detections was estimated to be 0.2 yr^{-1}, with an average of $\sim 20\ M_\oplus$ of material ejected per star [277]. The number density was estimated to be $n \sim 10^{-2}$ au^{-3} [278], implying a total number of $N \sim 2 \times 10^{26}$ throughout the Milky Way and a galactic mass of $M \sim 10^{11}\ M_\oplus$. A more detailed analysis that incorporated the survey sensitivities of observational facilities resulted in a number density $n \sim 2 \times 10^{-1}$ au^{-3} [279]. If we assume a mass of $M_{1I} = 10^{12}$ g in every 1I/'Oumuamua-like object, this implies a total galactic mass density of $0.3\ M_\oplus$ pc^{-3}. This translates to a population of $N \sim 4 \times 10^{26}$ in the Milky Way, or approximately $1\ M_\oplus$ per stellar system. Based on the non-detection of similar objects since these initial estimates, this number density has been revised to $n \sim 1 \times 10^{-1}$ au^{-3} [66,167]. Frustratingly, the detection of 2I/Borisov does not constrain the number density of interstellar objects due to its brightness and discovery method.

As mentioned above, the number density of interstellar objects is higher than expected, if we assume that 1I/'Oumuamua is representative of a population that is uniformly distributed. Population studies that have tackled this discrepancy have estimated the number density of interstellar planetesimals based on the observed number of stars per unit volume of space and an estimated number of ejected planetesimals per star.

4.1.1. Contribution from protoplanetary disks around single stars and close binaries

Feasible sources of planetesimal ejection are dynamical instabilities and orbit readjustment that occur as a result of interactions between planetesimal and growing planets. These interactions lead to planetary migration, as is thought to have occurred in the early Solar System [42,289]. Numerical simulations show that these episodes of dynamical instability and planetesimal ejection are common in many planetary configurations [139]. In the Solar System, there is evidence that the planetesimal belts were heavily depleted and that the primordial Kuiper and asteroid belts were significantly more massive. The two pieces of evidence are the existence of Kuiper belt objects larger than 200 km (which formation by pairwise accretion must have required a number density of objects about two orders of magnitude higher than today), and the strong depletion in the asteroid belt region with respect to the minimum mass solar nebula.

Ejection occurs when the giant planets in the Solar System have close encounters with planetesimals. Some of these close encounters would impart sufficient energy to eject the planetesimal. Based on theoretical models of the timing of giant planet migration and/or instability in the Solar System, it seems likely that this occurred within the first < 10 Myr after the disk dispersed [290–298]. Moreover, the recent report of an excess of free-floating planets in the newly formed (<10 Myr) Upper Scorpius stellar association [299] is consistent with ubiquitous early ejection of debris.

For a giant planet to eject an interstellar comet, the planet must impart sufficient energy via a close encounter to scatter the comet onto an unbound trajectory. The Safronov number $\Theta = V_e^2/(2V_K^2)$ is useful to quantify the efficiency of this process, where V_e is the escape

velocity and V_K is the orbital velocity. Only objects with $\Theta > 1$ are capable of ejecting objects. The Safronov number may be written as

$$\Theta = \left(\frac{M_P}{M_*}\right)\left(\frac{a_P}{R_P}\right). \quad (6)$$

In Equation (6), M_* and M_P are the mass of the star and planet, while a_P and R_P are the semimajor axis and radius of the planet. Because the ejection is more efficient beyond the snowline (as the Safronov number for a planet of a given mass increases with orbital distance), the majority of the ejected planetesimals are expected to be icy. However, objects subject to multiple close passages by their host star could be ejected from closer in [103]. In the Solar System, all of the giant planets have $\Theta > 1$ while the interior terrestrial planets have $\Theta < 1$. Therefore, the material ejected from the Solar System mostly came from the outer regions, with Jupiter and Neptune responsible for most of the ejections and the population of the Oort Cloud and Kuiper belt. It has been argued that if interstellar planetesimals come from a ubiquitous and isotropic distribution, it is possible that Jupiter and Neptune analogues are typical in extrasolar systems [278].

The estimate shown in Table 5 by [287] labelled *singles* corresponds to the contribution to the interstellar object population from the ejection of planetesimals from protoplanetary around single stars and close binaries, as a result of the planetesimal and planet formation process. In this calculation, it is assumed that the disk mass is 1% that of the stellar mass, that 1% is in the form of solids, and that most of the solids are ejected.

4.1.2. Contribution from circumbinary disks

Intriguingly, circumbinary systems can also be a source of ejected material. Importantly, this material would be ejected from much closer into the potential well of the system. This has implications for the composition of the ejected bodies. In [300], it was estimated that approximately ∼1/3 of the ejected material would be icy. The remaining fraction would have spent significant time close to the binary stars prior to ejection, becoming devolatised. This was used initially as an explanation for the lack of outgassing activity in 1I/'Oumuamua [300,301]. It is intriguing that some interstellar comets may come from circumbinary systems, and be representative of material that formed at closer stellocentric distances. Moreover, [302] demonstrated that *misaligned* circumbinary disks are even more efficient at ejecting interstellar comets.

The estimate shown in Table 5 labeled *binaries* [287] corresponds to interstellar objects ejected from circumbinary disks. This estimate assumes, based on [300], that the mass of the circumbinary disk is 10% of the binary system, that 10% of that material migrates due to gas drag and crosses the unstable radius at which point the objects are ejected, and that 1% of that material is solids.

4.1.3. Contribution from exo-Oort clouds

Another potential source of interstellar planetesimals are exo-Oort clouds. These are swarms of planetesimals that, like the Solar System Oort cloud, are thought to be weakly bound to the central star. The detection of these Oort clouds lies beyond our current observational capabilities, even for the Solar System Oort cloud. Based on the observed flux of LPCs in the Solar System, it is estimated that the Oort Cloud harbours $\sim 10^{12}$ objects larger than 2.3 km ([11] and references therein). Oort clouds are thought to be a source of interstellar planetesimals because, as the central star reaches the end of its lifetime, it loses mass in its transition to a white dwarf. This mass loss and the subsequent winds can release the weakly-bound Oort cloud objects into the interstellar medium [303–305]. Exo-Oort cloud objects can also be released via close encounters with other stars [306] or the galactic tide [307–309].

The estimate shown in Table 5 labelled *Oort cloud* [288] corresponds to the contribution to the interstellar object population from the release of these putative exo-Oort clouds. Because we lack exo-Oort cloud observations, it is not clear whether or not typical stars harbor exo-Oort clouds. A study by [47] found that the Oort cloud formation efficiency is similar at a wide range of Galactocentric distances. However, [310] found that the parameter space (in terms of planetary architecture) to form an Oort cloud is quite restricted. The estimate shown in Table 5 labelled *Oort Cloud* [288] adopts the simplifying assumption that exo-Oort clouds are ubiquitous, that they have a population similar to that of the Oort cloud, but scaled to the stellar mass, $10^{12} M_*/M_\odot$, and that they are located at distances similar to that of the Oort cloud, but scaled to Hill radius of its parent star in the Galactic potential. The calculation further assumes exo-Oort cloud clearing is caused by post-main sequence mass loss for stars with 1–8 $M_\odot$ and stellar encounters for stars that are still on their main sequence. It assumes varying ejection efficiencies as a function of the stellocentric distances based on previously published dynamical models [307–309].

However, these post-main sequence stars are necessarily old and have been subject to dynamical heating. Therefore, their ejected objects are expected to have very large velocities as they enter the Solar System. This contrasts with the low velocity of 1I/'Oumuamua, indicating that this object is unlikely to have originated as ejecta

from a post main-sequence system. The same is true for 2I/Borisov, given its hypervolatile composition.

There are many uncertainties in the calculations shown for the different potential sources. However, the population studies generally find that there is a discrepancy between the estimated number density of interstellar planetesimals and that inferred from the detection of 1I/'Oumuamua. This discrepancy indicates that there is much to learn about the population of interstellar planetesimals and their origin. One solution proposed by [287] could be that 1I/'Oumuamua was not representative of an isotropic distribution of interstellar planetesimals. This could be explained if the object originated in a nearby planetary system. As discussed below, this scenario would be consistent with 1I/'Oumuamua's kinematics.

4.2. Kinematics

The incoming velocities of interstellar objects provide critical information regarding their ages and galactic histories. However, meaningful interpretations of the kinematics of interstellar objects with regard to their provenance most likely will require a larger statistical sample.

In the Milky Way, gravitational interactions with Giant Molecular Clouds (GMCs) and other substrucutures tend to gradually increase the velocity dispersions of stars [311,312]. This process is colloquially referred to as dynamical heating and manifests most obviously in the out of plane z-component of galactic velocities. The thin disk of the Milky Way contains younger stars with lower z-dispersion, while older stars that have experienced more dynamical heating populate the thick disk and have larger excursions out of the galactic plane. Younger stars like B0 stars have typical dispersions of 10 s of $\mathrm{km\,s^{-1}}$, while older stellar populations exhibit higher dispersions [313]. Transient structures like GMCs are much younger and have much lower dispersions $\sim$1 $\mathrm{km\,s^{-1}}$ [314]. However, these estimates are complicated by a large systematic uncertainty in the velocity of the Sun with respect to the Local Standard of Rest (LSR) [315,316].

1I/'Oumuamua exhibited a surprisingly low hyperbolic velocity of 26 $\mathrm{km\ s^{-1}}$ when compared to the 15 ± 2 $\mathrm{km\,s^{-1}}$ velocity of the Sun relative to the LSR [317]. 2I/Borisov exhibited a larger relative velocity of 32 $\mathrm{km\,s^{-1}}$. This is indicative that 2I/Borisov has been subject to substantially more dynamical heating than 1I/'Oumuamua, which is presumably due to an older galactic age. The approximate dynamical ages of these objects have been inferred to be $\tau_s \sim 10^8$ years for 1I/'Oumuamua [317–320] and for 2I/Borisov $\tau_s \sim 10^9$ years [319]. It should be noted that these ages are only statistical in nature.

Another indicator of a young age for 1I/'Oumuamua is its suggested tumbling state with [73] hypothesising that the tumbling state could be related to a collision in its parent system. This would suggest that the object is younger than $\sim$1 Gyr, corresponding to the damping timescale due to stresses and strains resulting from complex rotation for an object with 1I/'Oumuamua's inferred properties. A recent ejection is also consistent with the fact that 1I/'Oumuamua's surface did not seem to be heavily processed based on its colour. As mentioned in Section 2.3.2, unlike the cold classical Kuiper belt objects that are ultra-red because of billions of years of exposure to cosmic rays, plasma and radiation, 1I/'Oumuamua's surface was not ultra-red.

4.3. Tracing interstellar objects to progenitor systems

The statistical nature of stellar dynamics makes it difficult to infer a home system for a single interstellar object based on the galactic kinematics. Moreover, the chaotic nature of the galactic motions and the uncertainty in stellar kinematic measurements complicates this task further. In [317], it was suggested that 1I/'Oumuamua's trajectory was sufficiently distinct from all local stars such that it was not co-moving with any single one and therefore not associated with any local exo-Oort clouds. However, [318] suggested that the kinematics of 1I/'Oumuamua pointed to its formation in a protoplanetary disk in the Carina or Columba young stellar associations.

Rigorous analysis of the galactic history of 1I/'Oumuamua concluded that it likely originated within 1 kpc of the Earth, based on its young dynamical age [319]. While identification of a home system is not possible, they reported that 1I/'Oumuamua likely passed through a large subset of the Carina and Columba moving groups at the time that those groups were forming. A similar set of dynamical simulations performed by [320] were consistent with these results, pointing towards formation within a Giant Molecular Cloud. As for 2I/Borisov, [319] demonstrated that identifying its home system is effectively impossible.

As pointed out earlier, it is critical to note that if 1I/'Oumuamua had a local origin, the implied $n \sim 0.1\ \mathrm{au^{-3}}$ number density based on its detection may not apply to the entire Galaxy. Furthermore, [287] argued that if 1I/'Oumuamua was ejected from a young nearby star, the spatial density may be highly anisotropic. This

would somewhat resolve the discrepancy between the expected number density of interstellar objects and that inferred from the detection of 1I/'Oumuamua which had assumed an isotropic distribution.

Other attempts to trace 1I/'Oumuamua to a home system were unsuccessful. In [321], the search for previous stellar close encounters with 1I/'Oumuamua resulted in none. They noted a ∼2.2 pc close encounter with the nearby planet-bearing star Gliese 876 [322], but this distance is too far to provide a definitive association. A different study by [323] broadened this analyses and identified 109 potential close encounters but no definitive home system. Another study by [324] presented a generalised method to estimate the probability that an interstellar object is associated with a stellar system, a methodology that should be useful when a statistical sample of interstellar object kinematics is available. They noted a slight association with the binary star system HD200325. Even with accurate stellar kinematics from the European Space Agency (ESA) mission Gaia [325–327] reported unlikely prospects to trace a single interstellar object to a host system.

4.4. Size-frequency distribution of interstellar comets

Constraining the size-frequency distribution of the galactic population of interstellar objects is difficult at the large end of the spectrum because there are only two detections of macroscopic interstellar objects. However, there is a long history of studies focusing on the size-frequency distribution of interstellar dust, showing a well-established power law. Extrapolations of these distributions are tentatively consistent with the implied occurrence rate of 1I/'Oumuamua [66], although caution should be used when extrapolating based on such small number statistics.

Measurements of interstellar dust date back to the Ulysses and Galileo spacecrafts. Combined cumulative results from both of these spacecrafts were reported in [328] and individual spacecraft measurements were reported in [329–331]. A controversial detection of an interstellar meteor with the Arecibo Observatory was reported in [332]. Subsequent radar measurements with the Arecibo UHF (430 MHz) were reported by [333,334]. The first radar-based detection of micron-sized hyperbolic meteors with the Advanced Meteor Orbit Radar (AMOR) was attributed to the debris-disk host star β Pic [335–337]. The lower limit from the Canadian Meteor Orbit Radar (CMOR) from 12 possible interstellar events from 1.5 million measured orbits were reported by [338].

At the larger end of the spectrum, [339] analysed the extant video data (multi-station photographic and television techniques) to constrain the flux of large interstellar meteoroids. An upper limit using optical data with the Canadian Automated Meteor Observatory (CAMO) was reported by [340]. An extensive analysis of the IAU Meteor Data Center photographic database showed that the vast majority of the apparent hyperbolic meteors were a consequence of measurement error [341,342].

These data are broadly compatible with a r_n^{-3} size distribution for interstellar particles, including for 1I/'Oumuamua and free-floating planets [66,288,343]. Larger particles in principle could produce interstellar meteors. These would have large excess velocities and trajectories with eccentricies $e > 1$. However, these interstellar meteors are notoriously difficult to identify because planetary perturbations can scatter particles onto hyperbolic trajectories [344,345]. Therefore, extremely precise measurements of the incoming velocity vector would be required to verify a meteor as interstellar [346]. Recently, there have been claims of interstellar meteors detected in the CNEOS database [347,348]. However, it is well established that these observations are susceptible to poor accuracy of data. The reported velocity vectors are most notoriously untrustworthy, which are instrumental in aquiring pre-impact trajectories and meteorite fall positions [349]. Moreover, the number of apparently hyperbolic events in databases, which have been routinely detected for decades, is used primarily as an estimation of the typical error in the detection method. The claims of the interstellar nature of meteorites are largely disproven due to the poor quality of the data and the nondisclosure of error bars [350].

As discussed in Section 4, the comparison of the expected mass budget of ejected planetesimals from extrasolar planetary systems, based on population studies, to the mass budget of interstellar planetesimals, inferred from the detection of 1I/'Oumuamua, shows a significant discrepancy [287]. A critical assumption in the calculation of the latter is the albedo and size of 1I/'Oumuamua, and the expected size distribution of interstellar objects. Given the large uncertainties in the latter, the size distribution that is adopted is based on the small body population of the Solar System. This allows for a wide range of possible values that define a broken power-law [287]. Even when adopting this wide range of values, the discrepancy in the mass budget is still present.

4.5. Captured interstellar objects in the Solar System?

It has been hypothesised that the Solar System could capture unbound objects from the Galaxy via its gravitational perturbations. This process requires some external force to modify the hyperbolic trajectory of an interstellar

object to make it bound by the Solar System. This capture process could be driven by external stellar flybys of the tidal galactic gravitational field. Alternatively, it may be driven by more localised perturbations from a Solar System planet. It has also been hypothesised that some of the Oort cloud comets in the Solar System were captured from other Oort clouds around other stars. This would require the tidal galactic field to impart torques on passing objects. This process may have been more efficient during the earliest phases of the formation of the Solar System, when it was in a birth cluster containing many stars [351]. More recent calculations have estimated that the Solar System harbors $\sim 10^7$ trapped 1I/'Oumuamua-size interstellar objects within $\sim$20,000 au [352].

The interstellar objects that pass interior to Neptune could in theory come close to one of the planets and be captured into the Solar System. Since the discovery of 1I/'Oumuamua, several studies have performed detailed calculations to quantify the effectiveness of this process [353,354]. By in large these studies agree that it is a relatively ineffective process, and only $\simeq 10^{-9} M_\oplus$ of interstellar material should be present in the Solar System [355]. With a different set of assumptions, [354] estimated that $\sim$8 captured interstellar objects would exist within 5 au of the Sun.

There was a claim that Centaurs and Trojans with high inclination, retrograde orbits were captured interstellar objects [356]. However, this was quickly disproved, when [357] pointed out that these objects are more likely to come from transient capture of Oort cloud comets. It therefore seems unlikely that captured interstellar objects will be detected in the Solar System.

4.6. Interstellar planetesimals seeding planet formation

A longstanding obstacle in the theory of planetary formation is the so-called 'meter barrier '. The formation of cm-sized particles is efficient and has been well studied [358,359]. At the metre size, however, collisions between particles have increasing collisional energies and are prone to trigger shattering events [360]. Moreover, these larger objects are subject to rapid inward drift timescales as the protostellar gas provides a drag force which removes angular momentum and causes the particles to quickly inspiral. This process significantly limits the lifetime of growing planetesimals in the disk. Several theoretical advances have been proposed to alleviate this problem: the streaming instability which rapidly agglomerates particles into larger objects on secular timescales [361]; the direct formation via gravitational instability [362]; the presence of low-velocity collisions in the velocity distribution of the dust particles, favouring growth [363]; the trapping of dust grains in pressure maxima [364]; and the effect of low porosity and the electric charging of dust aggregates to favour sticking over fragmentation [365,366].

The discovery of the first interstellar objects led to an additional proposal to alleviate the 'meter barrier': the capture of interstellar objects by gas drag into star- and planet-formation environments. This could occur during an early stage, when the objects are trapped into Giant Molecular Clouds. The captured objects tracing the collapse of the prestellar core may subsequently become incorporated into fragmenting star- and planet-forming regions [367,368]. Moreover, interstellar objects may also be captured by already formed protoplanetary disks [369]. These ideas were further explored by [370] who considered the efficiency of capturing and incorporating interstellar planetesimals into star- and planet-forming regions, as a function of their velocity dispersion, size distribution and number density. They found that, when assuming a background number density of $0.2\,\mathrm{au}^{-3}$ (derived from [279]), a velocity dispersion of $30\,\mathrm{km\,s}^{-1}$ (characteristic of the young stars in the Galaxy from where interstellar objects likely originated), and an equilibrium size distribution of $q' = 3.5$, the number of interstellar objects captured by a Giant Molecular Cloud and expected to be incorporated into each protoplanetary disk during their formation would be $\mathcal{O}(10^9)$ (50 cm–5 m), $\mathcal{O}(10^5)$ (5–50 m), $\mathcal{O}(10^2)$ (50–500 m), $\mathcal{O}(10^{-2})$ (500 m–5 km). During a later stage, when the protoplanetary disk is formed, the number of interstellar objects that could be captured from the interstellar medium during its lifetime would be $\mathcal{O}(10^{12})$ (50 cm–5 m), $\mathcal{O}(10^8)$ (5–50 m), $\mathcal{O}(10^5)$ (50–500 m), $\mathcal{O}(10^1)$ (500 m–5 km). In an open cluster where $\sim$1% of stars have undergone planet formation, these values would increase by a factor of $\mathcal{O}(10^2$–$10^3)$. These trapped interstellar objects might be large enough to rapidly grow into larger planetesimals via the direct accretion of the subcm-sized dust grains in the protoplanetary disk before they drift inwards due to gas drag. This provides a promising alternative avenue to overcome the metre barrier, with interstellar planetsimals acting as 'seeds' for planet formation.

The estimates above by [370] are very uncertain because, as discussed in Sections 4.1 and 4.4, the number density and velocity and size distribution of interstellar objects are uncertain. These estimates will be substantially refined as the population of interstellar objects becomes better characterised. However, these preliminary studies have shown that as the number density of interstellar planetesimals in the Galaxy increases with time, their trapping in star- and planet-formation environments may be significant. Therefore, future star- and

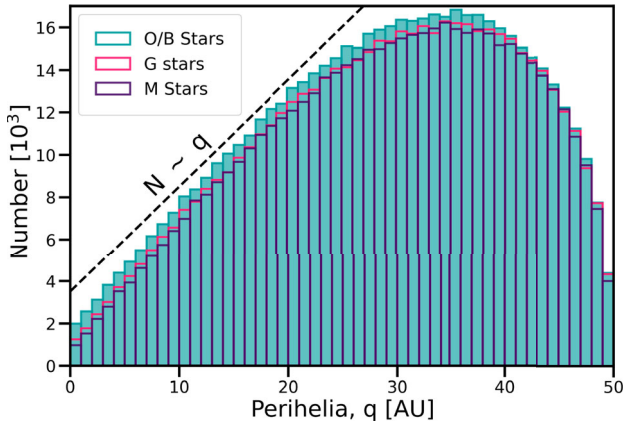

Figure 10. Predicted perihelia distribution of interstellar objects from the probabilistic method generated by [373]. Distributions are shown assuming incoming kinematics of various stellar populations. Reproduced with permission from [373].

planet-formation models should take into account the presence of this population of captured objects to assess if it can significantly influence planet formation, particularly in cluster environments.

5. Future prospects

5.1. Orbits of interstellar objects in the solar system

There has been significant interest in identifying the future prospects for the detection and characterisation of interstellar objects. As discussed previously (see Section 4.1), the discovery of 1I/'Oumuamua, if representative of an isotropically distributed population, might imply that a galactic population of similar objects exists with spatial number density of $n \sim 0.1\,\mathrm{au}^{-3}$. There has therefore been significant efforts invested into identifying the expected orbital distributions of interstellar objects that travel through the Solar System.

The kinematic distribution of local stars in the local stellar neighbourhood is well measured (see Section 4.2). Moreover, interstellar objects should represent a better realisation of the kinematics of the gravitational potential of the Milky Way since there are estimated to be orders of magnitude more of them than stars in the Galaxy. Assuming that the incoming interstellar objects trace this velocity distribution, the distribution of orbits expected for the interstellar objects that pass through the Solar System can be calculated.

This is straightforward to implement numerically via a Monte Carlo method. This was performed by [285,286] prior to the detection of 1I/'Oumuamua. After its discovery, with updated number densities, these simulations were re-performed and modified by [371,372]. With an elegant mathematical analysis, [373] provided an entirely analytic method to calculate the distribution of interstellar object orbits. They showed comparisons of their analytic method (which they label the probabilistic method)–with the numerical method previously performed (that they refer to as the dynamical method), demonstrating that the probabilistic method is orders of magnitude more computationally efficient and also more accurate. The resulting distribution of perihelia is shown in Figure 10, for interstellar comet populations with galactic velocity dispersions of various stellar populations. In all cases, the number of interstellar objects passing through the Solar System varies linearly with perihelia.

5.2. Ground-based prospects

The forthcoming Rubin Observatory Legacy Survey of Space and Time (LSST) [374,375] will be efficient at detecting transient objects [376–379]. Literature estimates based on survey detection efficiency and criteria and number densities estimate that the survey will detect $\sim$1–3 1I/'Oumuamua-like interstellar object per year [277,284–286,371–373].

The most recent study of the of the expected distribution of interstellar objects by [372] included a calculation of the distribution of orbital elements and close approaches to the Earth of interstellar objects that will be detected by the LSST. They incorporated a set of LSST detection criteria in this analysis that required that the elongation angle and phase be such that the LSST would be able to detect the object. The results of this simulation are shown in Table 6 and show that the LSST should detect 1–2 interstellar objects per year.

5.3. Space-based prospects

The forthcoming NEO Surveyor [380] may also detect interstellar objects. NEO Surveyor has a 50-cm diameter telescope and will be located interior to Earth's orbit at L1. The mission has been optimised to find small bodies out to Jupiter that could be potentially hazardous. Moreover, the mission will provide thermal infrared measurements of these objects. NEO Surveyor and possibly *JWST* will be able to characterise both the sizes and albedos of these objects.

Recently, ESA selected the *Comet Interceptor* [381] which will fly in 2029. *Comet Interceptor* has a low $\Delta V \sim 1\,\mathrm{km\,s}^{-1}$ budget, and is designed to rendezvous with an LPC. If an interstellar object is detected with a serendipitously fortuitous orbit, then it is possible that *Comet Interceptor* will reroute and rendezvous with it. For example, [371] showed that an impactor mission to 1I/'Oumuamua sent from Earth would have been

Table 6. The frequency that interstellar objects are detectable by the LSST and reachable with a range of ΔV criteria.

Criterion	Percent	Conservative rate per year	Optimistic rate per year
$m \leq 24$	$\sim$ 7.0%	$\sim$2.3	$\sim$4.6
Detectable with the LSST	$\sim$2.8%	$\sim$0.9	$\sim$1.9
Detectable, $\Delta V < 30$ km/s	$\sim$1.1%	$\sim$0.35	$\sim$0.7
Detectable, $\Delta V < 15$ km/s	$\sim$0.4%	$\sim$0.1	$\sim$0.3
Detectable, $\Delta V < 2$ km/s	0.002%	$\sim 7 \times 10^{-4}$	$\sim$0.001

Notes: These calculations assume that each interstellar object has the same absolute magnitude as that of 1I/'Oumuamua. Reproduced from [372].

achievable with a $\Delta V \sim 4\,\mathrm{km\,s^{-1}}$ impulse given an earlier detection and sufficient lead time. About 10–30% of the interstellar interlopers to be detected by the LSST (Table 6) should be reachable by a mission with $\Delta V < 15\,\mathrm{km\,s^{-1}}$ [372]. There has been ample work done to design such a dedicated mission to an interstellar object [371,381–396], and it seems likely that a handful of reachable targets will be detected.

The study of interstellar objects, still in its infancy, will experience a revolution with upcoming ground-based and space-based observations. These will not only help us understand the origin(s) of this new component of the interstellar medium and the clues it unveils regarding planet formation, but will also allow for the extraordinary opportunity to study a fragment from another planetary system at close-range.

Acknowledgments

We thank Dušan Marčeta for providing simulation results for Figure 10. We thank Davide Farnocchia and Marco Micheli for detailed reviews of the manuscript prior to submission. We thank Jennifer Bergner, Aster Taylor, Lisa Kaltenegger, Dave Jewitt, Adina Feinstein, Fred Adams, Dong Lai, Nikole Lewis, Greg Laughlin and Juliette Becker for useful suggestions and conversations.

Disclosure statement

No potential conflict of interest was reported by the author(s).

Funding

DZS acknowledges financial support from the National Science Foundation Grant No. AST-2107796, NASA Grant No. 80NSSC19K0444 and NASA Contract NNX17AL71A.

Notes on contributors

Darryl Z. Seligman completed his undergraduate degrees in Mathematics and Physics at the University of Pennsylvania in 2015 and his Ph.D. at Yale University in Astronomy in 2020. He was the TC Chamberlin Fellow at the University of Chicago Department of the Geophysical Sciences after completing his Ph.D. He is currently at Cornell and will be a Simonyi-NSF Scholar, an NSF Astronomy and Astrophysics Postdoctoral Fellowship award made in recognition of significant contributions to Rubin Observatory's Legacy Survey of Space and Time.

Amaya Moro-Martín received her PhD from the University of Arizona. She worked at Princeton University as a Michelson Fellow and as a Lyman Spitzer fellow, and at the Center for Astrobiology in Spain as a Ramon y Cajal fellow. Since 2014, she has worked at the Space Telescope Science Institute in the James Webb Space Telescope. Her scientific interests include solar and extrasolar circumstellar disks using observations and simulations. She is interested in the properties of the disks' planetesimal and dust populations and what they can tell us about the underlying planetary system architecture, the exchange of solid material between planetary systems, and the newly found interstellar planetesimals. The overarching goal is to shed light on the formation, evolution, and diversity of planetary systems, helping us place our solar system into context. She is an active science advocate and writes frequently about science funding and the need to bridge the gap between science and society.

References

[1] Yeomans DK. Comets. A chronological history of observation, science, myth, and folklore. 1st ed. NY, Wiley; 1991. https://ui.adsabs.harvard.edu/abs/1991ccho.book.....Y/abstract
[2] Halley E. A synopsis of the astronomy of comets. John Senex; 1705. Available from: https://library.si.edu/digital-library/book/synopsisofastron00hall.
[3] Kant I. Universal natural history and theory of the heavens or essay on the constitution and the mechanical origin of the whole universe according to newtonian principles (1755). Cambridge University Press; 2012.
[4] Lagrange JL. Sur l'origine des comètes. Vol. 74. Fuchs; 1812.
[5] Herschel W. Observations of a comet, with remarks on the construction of its different parts. Philos Trans R Soc Lond Ser I. 1812 Jan;102:115–143.
[6] Herschel W. Observations of a second comet, with remarks on its construction. Philos Trans R Soc Lond Ser I. 1812 Jan;102:229–237.
[7] des longitudes FB. Connaissance des temps ou des mouvements célestes, à l'usage des astronomes et des navigateurs. Gauthier-Villars; 1816. Available from: https://cdt.imcce.fr/items/show/165.
[8] Herschel W. On the proper motion of the Sun and Solar System; with an account of several changes that have happened among the fixed stars since the time of Mr.

Flamstead. by William Herschel, Esq. F. R. S. Philos Trans R Soc Lond Ser I. 1783 Jan;73:247–283.
[9] Oort JH. The structure of the cloud of comets surrounding the Solar System and a hypothesis concerning its origin. Bull Astron Inst Netherlands. 1950 Jan;11:91–110.
[10] Francis PJ. The demographics of long-period comets. ApJ. 2005 Dec;635(2):1348–1361.
[11] Brasser R, Morbidelli A. Oort cloud and scattered disc formation during a late dynamical instability in the Solar System. Icarus. 2013 Jul;225(1):40–49.
[12] Dones L, Brasser R, Kaib N, et al. Origin and evolution of the cometary reservoirs. Space Sci Rev. 2015 Dec;197(1–4):
191–269.
[13] Kaib NA, Quinn T. Reassessing the source of long-period comets. Science. 2009 Sep;325(5945):1234.
[14] Everhart E. The origin of short-period comets. ApJL. 1972 Jan;10:131.
[15] Vaghi S. The origin of Jupiter's family of comets. A&A. 1973 Apr;24:41.
[16] Joss PC. On the origin of short-period comets. A&A. 1973 Jun;25:271.
[17] Delsemme AH. Origin of the short-period comets. A&A. 1973 Dec;29:377.
[18] Prialnik D, Barucci MA, Young L. The trans-Neptunian Solar System. Elsevier; 2020. https://ui.adsabs.harvard.edu/abs/2020tnss.book.....P
[19] Leonard FC. The new planet pluto. Leaflet Astron Soc Pacific. 1930 Jan;1(30):121.
[20] Edgeworth KE. The evolution of our planetary system. J Br Astron Assoc. 1943 Jul;53:181–188.
[21] Edgeworth KE. The origin and evolution of the Solar System. MNRAS. 1949 Jan;109:600–609.
[22] Kuiper GP. On the origin of the Solar System. Proc Nat Acad Sci. 1951 Jan;37(1):1–14.
[23] Cameron AGW. The formation of the sun and planets. Icarus. 1962 Jan;1(1):13–69.
[24] Whipple FL. Evidence for a comet belt beyond Neptune. Proc Nat Acad Sci. 1964 May;51(5):711–718.
[25] Fernandez JA. On the existence of a comet belt beyond Neptune. MNRAS. 1980 Aug;192:481–491.
[26] Duncan M, Quinn T, Tremaine S. The origin of short-period comets. ApJL. 1988 May;328:L69.
[27] Quinn T, Tremaine S, Duncan M. Planetary perturbations and the origin of short-period comets. ApJ. 1990 Jun;355:667.
[28] Jewitt D, Luu J. Discovery of the candidate Kuiper belt object 1992 QB_1. Nature. 1993 Apr;362(6422):730–732.
[29] Elliot JL, Kern SD, Clancy KB, et al. The deep ecliptic survey: a search for Kuiper belt objects and centaurs. II. dynamical classification, the Kuiper belt plane, and the core population. AJ. 2005 Feb;129(2):1117–1162.
[30] Volk K, Murray-Clay R, Gladman B, et al. OSSOS III–resonant trans-Neptunian populations: constraints from the first quarter of the Outer Solar System Origins Survey. AJ. 2016 Jul;152(1):23.
[31] Shankman C, Kavelaars J, Gladman BJ, et al. OSSOS. II. A sharp transition in the absolute magnitude distribution of the Kuiper Belt's scattering population. AJ. 2016 Feb;151(2):31.
[32] Shankman C, Kavelaars JJ, Bannister MT, et al. OSSOS. VI. Striking biases in the detection of large semimajor axis trans-Neptunian objects. AJ. 2017 Aug;154(2):
50.
[33] Bannister MT, Gladman BJ, Kavelaars JJ, et al. OSSOS. VII. 800+ trans-Neptunian objects–the complete data release. ApJS. 2018 May;236(1):18.
[34] Hahn G, Bailey ME. Rapid dynamical evolution of giant comet Chiron. Nature. 1990 Nov;348:132–136.
[35] Levison HF, Duncan MJ. From the Kuiper belt to Jupiter-family comets: the spatial distribution of ecliptic comets. Icarus. 1997 May;127(1):13–32.
[36] Tiscareno MS, Malhotra R. The dynamics of known centaurs. AJ. 2003 Dec;126(6):3122–3131.
[37] Di Sisto RP, Brunini A. The origin and distribution of the Centaur population. Icarus. 2007 Sep;190(1):224–235.
[38] Bailey BL, Malhotra R. Two dynamical classes of Centaurs. Icarus. 2009 Sep;203(1):155–163.
[39] Sarid G, Volk K, Steckloff JK, et al. 29P/Schwassmann-Wachmann 1, A Centaur in the gateway to the Jupiter-family comets. ApJL. 2019 Sep;883(1):L25.
[40] Steckloff JK, Sarid G, Volk K, et al. P/2019 LD2 (ATLAS): an active centaur in imminent transition to the Jupiter family. ApJL. 2020 Dec;904(2):L20.
[41] Di Sisto RP, Rossignoli NL. Centaur and giant planet crossing populations: origin and distribution. Celestial Mech Dyn Astron. 2020 Jul;132(6-7):36.
[42] Nesvorný D. Dynamical evolution of the early Solar System. ARA&A. 2018 Sep;56:137–174.
[43] Tsiganis K, Gomes R, Morbidelli A, et al. Origin of the orbital architecture of the giant planets of the Solar System. Nature. 2005 May;435(7041):459–461.
[44] Morbidelli A, Levison HF, Tsiganis K, et al. Chaotic capture of Jupiter's Trojan asteroids in the early Solar System. Nature. 2005 May;435(7041):462–465.
[45] Hahn JM, Malhotra R. Orbital evolution of planets embedded in a planetesimal disk. AJ. 1999 Jun;117(6):
3041–3053.
[46] Gomes RS, Morbidelli A, Levison HF. Planetary migration in a planetesimal disk: why did Neptune stop at 30 AU?. Icarus. 2004 Aug;170(2):492–507.
[47] Brasser R, Higuchi A, Kaib N. Oort cloud formation at various Galactic distances. A&A. 2010 Jun;516:
A72.
[48] Higuchi A, Kokubo E. Effect of stellar encounters on comet cloud formation. AJ. 2015 Jul;150(1):26.
[49] Whipple FL. A comet model. I. The acceleration of comet Encke. ApJ. 1950 Mar;111:375–394.
[50] Whipple FL. A comet model. II. Physical relations for comets and meteors. ApJ. 1951 May;113:464.
[51] Marsden BG, Sekanina Z, Yeomans DK. Comets and nongravitational forces. V. AJ. 1973 Mar;78:211.
[52] Rickman H. Cometary dynamics. In: Souchay J, Dvorak R, editors. Lecture notes in Physics, Berlin Springer Verlag. Vol. 790. Springer; 2010. p. 341–399.
[53] Cochran AL, Levasseur-Regourd AC, Cordiner M, et al. The composition of comets. Space Sci Rev. 2015 Dec;197(1-4):9–46.
[54] Biver N, Bockelée-Morvan D. Chemical diversity in the comet population. IAU Focus Meet. 2016 Oct;29A:
228–232.
[55] Bockelée-Morvan D, Biver N. The composition of cometary ices. Philos Trans R Soc Lond Ser A. 2017 May;375(2097):Article ID 20160252.

[56] Harrington Pinto O, Womack M, Fernandez Y, et al. A survey of CO, CO_2, and H_2O in comets and centaurs. Planet Sci J. 2022 Nov;3(11):247.
[57] Bockelée-Morvan D, Biver N, Schambeau CA, et al. Water, hydrogen cyanide, carbon monoxide, and dust production from distant comet 29P/Schwassmann-Wachmann 1. A&A. 2022 Aug;664:A95.
[58] McKay AJ, DiSanti MA, Kelley MSP, et al. The peculiar volatile composition of CO-dominated comet C/2016 R2 (PanSTARRS). AJ. 2019 Sep;158(3):128.
[59] Seligman DZ, Rogers LA, Cabot SHC, et al. The volatile carbon-to-oxygen ratio as a tracer for the formation locations of interstellar comets. Planet Sci J. 2022 Jul;3(7):150.
[60] Ootsubo T, Kawakita H, Hamada S, et al. AKARI near-infrared spectroscopic survey for CO_2 in 18 comets. ApJ. 2012 Jun;752(1):15.
[61] A'Hearn MF, Feaga LM, Keller HU, et al. Cometary volatiles and the origin of comets. ApJ. 2012 Oct;758(1):29.
[62] Williams GV, Sato H, Sarneczky K, et al. Minor planets 2017 SN_33 and 2017 u1. Central Bureau Electron Tel. 2017 Oct;4450:1.
[63] Chambers KC, Magnier EA, Metcalfe N, et al. The Pan-STARRS1 surveys. arXiv e-prints. 2016 Dec.
[64] Wright JT. On distinguishing interstellar objects like 'Oumuamua from products of Solar System scattering. Res Notes Am Astron Soc. 2017 Dec;1(1):38.
[65] Schneider J. Is 1I/2017 U1 really of interstellar origin?. Res Notes Am Astron Soc. 2017 Dec;1(1):18.
[66] Jewitt D, Seligman DZ. The interstellar interlopers. arXiv e-prints. 2022 Sep. arXiv:2209.08182.
[67] Moro-Martín A. Interstellar planetesimals. arXiv e-prints. 2022 May. arXiv:2205.04277.
[68] Jewitt D, Luu J, Rajagopal J, et al. Interstellar interloper 1I/2017 U1: observations from the NOT and WIYN telescopes. ApJL. 2017 Dec;850:L36.
[69] Masiero J. Palomar optical spectrum of hyperbolic near-earth Object A/2017 U1. arXiv e-prints. 2017 Oct.
[70] Ye QZ, Zhang Q, Kelley MSP, et al. 1I/2017 U1 ('Oumuamua) is hot: imaging, spectroscopy, and search of meteor activity. ApJL. 2017 Dec;851:L5.
[71] Meech KJ, Weryk R, Micheli M, et al. A brief visit from a red and extremely elongated interstellar asteroid. Nature. 2017 Dec;552:378–381.
[72] Fitzsimmons A, Snodgrass C, Rozitis B, et al. Spectroscopy and thermal modelling of the first interstellar object 1I/2017 U1 'Oumuamua. Nat Astron. 2018 Dec;2:133–137.
[73] Drahus M, Guzik P, Waniak W, et al. Tumbling motion of 1I/'Oumuamua and its implications for the body's distant past. Nat Astron. 2018 May;2:407–412.
[74] Bannister MT, Schwamb ME, Fraser WC, et al. ColOSSOS: colors of the interstellar planetesimal 1I/'Oumuamua. ApJL. 2017 Dec;851(2):L38.
[75] Bolin BT, Weaver HA, Fernandez YR, et al. APO time-resolved color photometry of highly elongated interstellar object 1I/'Oumuamua. ApJL. 2018 Jan;852(1):L2.
[76] Knight MM, Protopapa S, Kelley MSP, et al. On the rotation period and shape of the hyperbolic asteroid 1I/'Oumuamua (2017 U1) from its lightcurve. ApJL. 2017 Dec;851(2):L31.
[77] Belton MJS, Hainaut OR, Meech KJ, et al. The excited spin state of 1I/2017 U1 'Oumuamua. ApJL. 2018 Apr;856:L21.
[78] Fraser WC, Pravec P, Fitzsimmons A, et al. The tumbling rotational state of 1I/'Oumuamua. Nat Astron. 2018 Feb;2:383–386.
[79] Park RS, Pisano DJ, Lazio TJW, et al. Search for OH 18 cm radio emission from 1I/2017 U1 with the Green bank telescope. AJ. 2018 May;155:185.
[80] Trilling DE, Mommert M, Hora JL, et al. Spitzer observations of interstellar object 1I/'Oumuamua. AJ. 2018 Dec;156:261.
[81] Seligman DZ, Levine WG, Cabot SHC, et al. On the spin dynamics of elongated minor bodies with applications to a possible Solar System analogue composition for 'Oumuamua. ApJ. 2021 Oct;920(1):28.
[82] Hui MT, Knight MM. New insights into interstellar object 1I/2017 u1 ('Oumuamua) from SOHO/STEREO nondetections. AJ. 2019 Dec;158(6):256.
[83] Enriquez JE, Siemion A, Lazio TJW, et al. Breakthrough listen observations of 1I/Oumuamua with the GBT. Res Notes Am Astron Soc. 2018 Jan;2(1):9.
[84] Tingay SJ, Kaplan DL, Lenc E, et al. A serendipitous MWA search for narrowband signals from 'Oumuamua. ApJ. 2018 Apr;857(1):11.
[85] Harp GR, Richards J, Jenniskens P, et al. Radio SETI observations of the interstellar object 'OUMUAMUA. Acta Astronaut. 2019 Feb;155:51–54.
[86] Pravec P, Harris AW. Binary asteroid population. 1. Angular momentum content. Icarus. 2007 Sep;190(1):250–259.
[87] Buratti BJ, Hofgartner JD, Hicks MD, et al. Global albedos of Pluto and Charon from LORRI new horizons observations. Icarus. 2017 May;287:207–217.
[88] Brown ME. The inclination distribution of the Kuiper belt. AJ. 2001 May;121(5):2804–2814.
[89] Gulbis AAS, Elliot JL, Adams ER, et al. Unbiased inclination distributions for objects in the Kuiper belt. AJ. 2010 Aug;140(2):350–369.
[90] Hainaut OR, Boehnhardt H, Protopapa S. Colours of minor bodies in the outer solar system. II. A statistical analysis revisited. A&A. 2012 Oct;546:A115.
[91] Jewitt D. Color systematics of comets and related bodies. AJ. 2015 Dec;150(6):201.
[92] Jewitt D. The Trojan color conundrum. AJ. 2018 Feb;155(2):56.
[93] Ostro SJ, Hudson RS, Nolan MC, et al. Radar observations of Asteroid 216 Kleopatra. Science. 2000 May;288(5467):836–839.
[94] Ostro SJ, Pravec P, Benner LAM, et al. Radar and optical observations of asteroid 1998 KY26. Science. 1999 Jun;285:557–559.
[95] Heinze A. A photometric analog for 'Oumuamua in our solar system. In: AAS/Division for Planetary Sciences Meeting Abstracts; (AAS/Division for Planetary Sciences Meeting Abstracts; Vol. 53); Oct.; 2021. p. 505.01.
[96] Licandro J, Popescu M, Tatsumi E, et al. Observations of two super fast rotator NEAs: 2021 NY_1 and 2022 AB. MNRAS. 2023 Mar. https://ui.adsabs.harvard.edu/abs/2023MNRAS.tmp..693L/abstract

[97] McNeill A, Trilling DE, Mommert M. Constraints on the density and internal strength of 1I/'Oumuamua. ApJL. 2018 Apr;857:L1.
[98] Mashchenko S. Modelling the light curve of 'Oumuamua: evidence for torque and disc-like shape. MNRAS. 2019 Nov;489(3):3003–3021.
[99] Domokos G, et al. Formation of sharp edges and planar areas of asteroids by polyhedral abrasion. ApJL. 2009 Jul;699(1):L13–L16.
[100] Domokos G, et al. Explaining the elongated shape of 'Oumuamua by the Eikonal abrasion model. RNAAS. 2017 Dec;1(1):50.
[101] Vavilov DE, Medvedev YD. Dust bombardment can explain the extremely elongated shape of 1I/'Oumuamua and the lack of interstellar objects. MNRAS. 2019 Mar;484(1):L75–L78.
[102] Sugiura K, Kobayashi H, Inutsuka S. Collisional elongation: possible origin of extremely elongated shape of 1I/'Oumuamua. Icarus. 2019 Aug;328:14–22.
[103] Raymond SN, Armitage PJ, Veras D. Interstellar object 'Oumuamua as an extinct fragment of an ejected cometary planetesimal. ApJL. 2018 Mar;856(1):L7.
[104] Zhang Y, Lin DNC. Tidal fragmentation as the origin of 1I/2017 U1 ('Oumuamua). Nat Astron. 2020 Apr;4:852–860.
[105] Moro-Martín A. Could 1i/'oumuamua be an icy fractal aggregate?. ApJL. 2019;872(2):L32.
[106] Zhou WH, Liu SF, Zhang Y, et al. Observable tests for the light-sail scenario of interstellar objects. A&A. 2022 Nov;667:A108.
[107] Vazan A, Sari R. On the aspect ratio of 'Oumuamua: less elongated shape for irregular surface properties. MNRAS. 2020 Feb. https://ui.adsabs.harvard.edu/abs/2020MNRAS.tmp..271V
[108] Micheli M, Farnocchia D, Meech KJ, et al. Non-gravitational acceleration in the trajectory of 1I/2017 U1 ('Oumuamua). Nature. 2018 Jun;559:223–226.
[109] Vokrouhlický D, Bottke WF, Chesley SR, et al. The Yarkovsky and YORP effects. In: Asteroids IV; 2015. p. 509–531.
[110] Vokrouhlický D, Milani A. Direct solar radiation pressure on the orbits of small near-Earth asteroids: observable effects?. A&A. 2000 Oct;362:746–755.
[111] Micheli M, Tholen DJ, Elliott GT. Detection of radiation pressure acting on 2009 BD. New A. 2012 May;17(4):446–452.
[112] Micheli M, Tholen DJ, Elliott GT. 2012 LA, an optimal astrometric target for radiation pressure detection. Icarus. 2013 Sep;226(1):251–255.
[113] Micheli M, Tholen DJ, Elliott GT. Radiation pressure detection and density estimate for 2011 MD. ApJL. 2014 Jun;788(1):L1.
[114] Mommert M, Hora JL, Farnocchia D, et al. Constraining the physical properties of near-Earth object 2009 BD. ApJ. 2014 May;786(2):148.
[115] Mommert M, Farnocchia D, Hora JL, et al. Physical properties of near-Earth asteroid 2011 MD. ApJL. 2014 Jul;789(1):L22.
[116] Farnocchia D, Tholen DJ, Micheli M, et al. Mass estimate and close approaches of near-Earth asteroid 2015 TC25. In: AAS/Division for Planetary Sciences Meeting Abstracts #49; Oct.; 2017. p. 100.09.
[117] Fedorets G, Micheli M, Jedicke R, et al. Establishing Earth's minimoon population through characterization of asteroid 2020 CD_3. AJ. 2020 Dec;160(6):277.
[118] Sekanina Z. 1I/'oumuamua as debris of dwarf interstellar comet that disintegrated before perihelion. arXiv e-prints. 2019 Jan. arXiv:1901.08704.
[119] Luu JX, Flekkøy EG, Toussaint R. 'Oumuamua as a cometary fractal aggregate: the 'Dust Bunny' model. ApJL. 2020 Sep;900(2):L22.
[120] Bialy S, Loeb A. Could Solar radiation pressure explain 'Oumuamua's peculiar acceleration?. ApJL. 2018 Nov;868(1):L1.
[121] Witten JTA, Sander LM. Diffusion-limited aggregation, a kinetic critical phenomenon. PRL. 1981 Nov;47(19):1400–1403.
[122] Suyama T, Wada K, Tanaka H. Numerical simulation of density evolution of dust aggregates in protoplanetary disks. I. Head-on collisions. ApJ. 2008 Sep;684(2):1310–1322.
[123] Okuzumi S, Tanaka H, Kobayashi H, et al. Rapid coagulation of porous dust aggregates outside the snow line: A pathway to successful icy planetesimal formation. ApJ. 2012 Jun;752(2):106.
[124] Kataoka A. Dust coagulation with porosity evolution. In: Pessah M, Gressel O, editors. Formation, evolution, and dynamics of young solar systems; (astrophysics and space science library; Vol. 445); Jan.; 2017. p. 143.
[125] Fulle M, Della Corte V, Rotundi A, et al. Density and charge of pristine fluffy particles from comet 67P/Churyumov-Gerasimenko. ApJL. 2015 Mar;802(1):L12.
[126] Mannel T, Bentley MS, Schmied R, et al. Fractal cometary dust – a window into the early Solar System. MNRAS. 2016 Nov;462:S304–S311.
[127] Flekkøy EG, Luu J, Toussaint R. The interstellar object 'Oumuamua as a fractal dust aggregate. ApJL. 2019 Nov;885(2):L41.
[128] Shoemaker CS, Shoemaker EM, Levy DH, et al. Comet Shoemaker-Levy (1993e). iaucirc. 1993 Mar;5725:1.
[129] Weaver HA, A'Hearn MF, Arpigny C, et al. The Hubble space telescope (HST) observing campaign on comet Shoemaker-Levy 9. Science. 1995 Mar;267(5202):1282–1288.
[130] Lellouch E, Paubert G, Moreno R, et al. Chemical and thermal response of Jupiter's atmosphere following the impact of comet Shoemaker-Levy 9. Nature. 1995 Feb;373(6515):592–595.
[131] Noll KS, McGrath MA, Trafton LM, et al. HST spectroscopic observations of Jupiter after the collision of comet Shoemaker-Levy 9. Science. 1995 Mar;267(5202):1307–1313.
[132] Schenk PM, Asphaug E, McKinnon WB, et al. Cometary nuclei and tidal disruption: the geologic record of crater chains on callisto and ganymede. Icarus. 1996 Jun;121(2):249–274.
[133] Melosh HJ, Stansberry JA. Doublet craters and the tidal disruption of binary asteroids. Icarus. 1991 Nov;94(1):171–179.

[134] Bottke WF, Melosh HJ. Formation of asteroid satellites and doublet craters by planetary tidal forces. Nature. 1996 May;381(6577):51–53.
[135] Bottke J, William F, Melosh HJ. Binary asteroids and the formation of doublet craters. Icarus. 1996 Dec;124(2):372–391.
[136] Melosh HJ, Ingram J, Bottke WF. The abundance of doublet craters on Mars. In: Lunar and Planetary Science Conference; (Lunar and Planetary Science Conference; Vol. 27); Mar.; 1996. p. 863.
[137] Cook CM, Melosh HJ, Bottke WF. Doublet craters on Venus. Icarus. 2003 Sep;165(1):90–100.
[138] Richardson DC, Bottke WF, Love SG. Tidal distortion and disruption of Earth-crossing asteroids. Icarus. 1998 Jul;134(1):47–76.
[139] Raymond SN, Armitage PJ, Veras D, et al. Implications of the interstellar object 1I/'Oumuamua for planetary dynamics and planetesimal formation. MNRAS. 2018 May;476(3):3031–3038.
[140] Raymond SN, Kaib NA, Armitage PJ, et al. Survivor bias: divergent fates of the Solar System's ejected versus persisting planetesimals. ApJL. 2020 Nov;904(1):L4.
[141] Taylor AG, Seligman DZ, MacAyeal DR, et al. Assessing potential contributions from outgassing and tidal effects on the evolving rotational state of 1I/'Oumuamua. arXiv e-prints. 2022 Sep. arXiv:2209.15074.
[142] Rafikov RR. Spin evolution and cometary interpretation of the interstellar minor object 1I/2017 'Oumuamua. ApJL. 2018 Nov;867:L17.
[143] Seligman D, Laughlin G, Batygin K. On the anomalous acceleration of 1I/2017 u1 'Oumuamua. ApJL. 2019 May;876:L26.
[144] Jewitt D, Sheppard S, Fernández Y. 143P/Kowal-Mrkos and the shapes of cometary nuclei. AJ. 2003 Jun;125(6):3366–3377.
[145] Drahus M, Jewitt D, Guilbert-Lepoutre A, et al. Rotation state of comet 103P/Hartley 2 from radio spectroscopy at 1 mm. ApJL. 2011 Jun;734(1):L4.
[146] Gicquel A, Bockelée-Morvan D, Zakharov VV, et al. Investigation of dust and water ice in comet 9P/Tempel 1 from Spitzer observations of the deep impact event. A&A. 2012 Jun;542:A119.
[147] Maquet L, Colas F, Jorda L, et al. CONGO, model of cometary non-gravitational forces combining astrometric and production rate data. Application to comet 19P/Borrelly. A&A. 2012 Dec;548:A81.
[148] Fernández YR, Kelley MS, Lamy PL, et al. Thermal properties, sizes, and size distribution of Jupiter-family cometary nuclei. Icarus. 2013 Sep;226(1):1138–1170.
[149] Wilson TG, Rawlings JMC, Swinyard BM. Herschel/SPIRE observations of water production rates and ortho-to-para ratios in comets. MNRAS. 2017 Apr;466(2):1954–1962.
[150] Eisner N, Knight MM, Schleicher DG. The rotation and other properties of comet 49P/Arend-Rigaux, 1984–2012. AJ. 2017 Nov;154(5):196.
[151] Roth NX, Gibb EL, Bonev BP, et al. A tale of 'Two' comets: the primary volatile composition of comet 2P/Encke across apparitions and implications for cometary science. AJ. 2018 Dec;156(6):251.
[152] Kokotanekova R, Snodgrass C, Lacerda P, et al. Implications of the small spin changes measured for large Jupiter-family comet nuclei. MNRAS. 2018 Oct;479(4):4665–4680.
[153] Biver N, Bockelée-Morvan D, Hofstadter M, et al. Long-term monitoring of the outgassing and composition of comet 67P/Churyumov-Gerasimenko with the Rosetta/MIRO instrument. A&A. 2019 Oct;630:A19.
[154] Combi MR, Mäkinen T, Bertaux JL, et al. Comet 41P/Tuttle-Giacobini-Kresak, 45P/Honda-Mrkos-Pajdusakova, and 46P/Wirtanen: water production activity over 21 yr with SOHO/SWAN. Planet Sci J. 2020 Dec;1(3):72.
[155] Jewitt D. Systematics and consequences of comet nucleus outgassing torques. AJ. 2021 Jun;161(6):261.
[156] Jewitt D. Destruction of long-period comets. AJ. 2022 Oct;164(4):158.
[157] Sekanina Z. Outgassing as trigger of 1I/'Oumuamua's nongravitational acceleration: could this hypothesis work at all? arXiv e-prints. 2019 May. arXiv:1905.00935.
[158] Seligman D, Laughlin G. Evidence that 1I/2017 U1 ('Oumuamua) was composed of molecular hydrogen ice. ApJL. 2020 Jun;896(1):L8.
[159] Britt DT, Consolmagno GJ, Merline WJ. Small body density and porosity: new data, new insights. In: Mackwell S, Stansbery E, editors. 37th Annual Lunar and Planetary Science Conference; Mar.; 2006. p. 2214; Lunar and Planetary Science Conference.
[160] Steckloff JK, Lisse CM, Safrit TK, et al. The sublimative evolution of (486,958) Arrokoth. Icarus. 2021 Mar;356:113998.
[161] Füglistaler A, Pfenniger D. Solid H_2 in the interstellar medium. A&A. 2018 Jun;613:A64.
[162] Hoang T, Loeb A. Destruction of molecular hydrogen ice and implications for 1I/2017 U1 ('Oumuamua). ApJL. 2020 Aug;899(2):L23.
[163] Phan VHM, Hoang T, Loeb A. Erosion of icy interstellar objects by cosmic rays and implications for 'oumuamua. arXiv e-prints. Sep 2021. arXiv:2109.04494.
[164] Levine WG, Laughlin G. Assessing the formation of solid hydrogen objects in starless molecular cloud cores. ApJ. 2021 May;912(1):3.
[165] Jackson AP, Desch SJ. 1i/'oumuamua as an n2 ice fragment of an exo-pluto surface: I. size and compositional constraints. J Geophys Res Planets. 2021;126:e2020JE006706.
[166] Desch SJ, Jackson AP. 1i/'oumuamua as an n2 ice fragment of an exo-pluto surface II: generation of N2 ice fragments and the origin of 'Oumuamua. J Geophys Res Planets. 2021;e2020JE006807.
[167] Levine WG, Cabot SHC, Seligman D, et al. Constraints on the occurrence of 'Oumuamua-Like objects. ApJ. 2021 Nov;922(1):39.
[168] Desch SJ, Jackson AP. Some pertinent issues for interstellar panspermia raised after the discovery of 1I/'Oumuamua. Astrobiology. 2022 Dec;22(12):1400–1413.
[169] Gasc S, Altwegg K, Balsiger H, et al. Change of outgassing pattern of 67P/Churyumov-Gerasimenko during the March 2016 equinox as seen by ROSINA. MNRAS. 2017 Jul;469:S108–S117.
[170] Bergner JB, Seligman DZ. Acceleration of 1i/'oumuamua from radiolytically produced h2 in h2o ice. Nature. 2023

Mar;615(7953):610–613. DOI:10.1038/s41586-022-05687-w
[171] Bar-Nun A, Herman G, Rappaport ML, et al. Ejection of H_2O, O_2, H_2 and H from water ice by 0.5–6 keV H^+ and Ne^+ ion bombardment. Surf Sci. 1985 Feb;150(1):143–156.
[172] Sandford SA, Allamandola LJ. H2 in interstellar and extragalactic ices: infrared characteristics, ultraviolet production, and implications. ApJL. 1993 Jun;409:L65.
[173] Watanabe N, Horii T, Kouchi A. Measurements of D_2 yields from amorphous D_2O ice by ultraviolet irradiation at 12 K. ApJ. 2000 Oct;541(2):772–778.
[174] Grieves GA, Orlando TM. The importance of pores in the electron stimulated production of D_2 and O_2 in low temperature ice. Surf Sci. 2005 Nov;593(1–3):180–186.
[175] Zheng W, Jewitt D, Kaiser RI. Formation of hydrogen, oxygen, and hydrogen peroxide in electron-irradiated crystalline water ice. ApJ. 2006 Mar;639(1):534–548.
[176] Zheng W, Jewitt D, Kaiser RI. Temperature dependence of the formation of hydrogen, oxygen, and hydrogen peroxide in electron-irradiated crystalline water ice. ApJ. 2006 Sep;648(1):753–761.
[177] Zheng W, Jewitt D, Kaiser RI. Electron irradiation of crystalline and amorphous D $_2$O ice. Chem Phys Lett. 2007 Feb;435(4):289–294.
[178] Bar-Nun A, Prialnik D. The possible formation of a hydrogen coma around comets at large heliocentric distances. ApJL. 1988 Jan;324:L31.
[179] Maggiolo R, Gronoff G, Cessateur G, et al. The effect of cosmic rays on cometary nuclei. II. Impact on ice composition and structure. ApJ. 2020 Oct;901(2):136.
[180] Gronoff G, Maggiolo R, Cessateur G, et al. The effect of cosmic rays on cometary nuclei. I. Dose deposition. ApJ. 2020 Feb;890(1):89.
[181] Stern S. Ism-induced erosion and gas-dynamical drag in the oort cloud. Icarus. 1990;84(2):447–466.
[182] Jewitt D. The active asteroids. AJ. 2012 Mar;143(3):66.
[183] Hsieh HH. Asteroid-comet continuum objects in the solar system. Philos Trans R Soc Lond Ser A. 2017 May;375(2097):Article ID 20160259.
[184] Jewitt D, Hsieh HH. The asteroid-comet continuum. arXiv e-prints. Mar 2022. arXiv:2203.01397.
[185] Hsieh HH, Jewitt D. A population of comets in the main asteroid belt. Science. 2006 Apr;312(5773):561–563.
[186] Elst EW, Pizarro O, Pollas C, et al. Comet P/1996 N2 (Elst-Pizarro). IAUCirc. 1996 Aug;6456:1.
[187] Boehnhardt H, Schulz R, Tozzi GP, et al. Comet P/1996 N2 (Elst-Pizarro). IAUCirc. 1996 Oct;6495:2.
[188] Toth I. Impact-generated activity period of the asteroid 7968 Elst-Pizarro in 1996: identification of the asteroid 427 Galene as the most probable parent body of the impactors. A&A. 2000 Aug;360:375–380.
[189] Hsieh HH, Jewitt DC, Fernández YR. The strange case of 133P/Elst-Pizarro: a comet among the asteroids. AJ. 2004 May;127(5):2997–3017.
[190] Sonnett S, Kleyna J, Jedicke R, et al. Limits on the size and orbit distribution of main belt comets. Icarus. 2011 Oct;215(2):534–546.
[191] Bertini I. Main belt comets: A new class of small bodies in the solar system. Planet Space Sci. 2011 Apr;59(5–6):365–377.
[192] Snodgrass C, Agarwal J, Combi M, et al. The main belt comets and ice in the Solar System. A&A Rev. 2017 Nov;25(1):5.
[193] Ferellec L, Snodgrass C, Fitzsimmons A, et al. A targeted search for main belt comets. MNRAS. 2022 Nov.
[194] Hui MT, Jewitt D. Non-gravitational acceleration of the active asteroids. AJ. 2017 Feb;153(2):80.
[195] Snodgrass C, Tubiana C, Vincent JB, et al. A collision in 2009 as the origin of the debris trail of asteroid P/2010A2. Nature. 2010 Oct;467(7317):814–816.
[196] Jewitt D, Agarwal J, Li J, et al. Disintegrating asteroid P/2013 R3. ApJL. 2014 Mar;784(1):L8.
[197] Gustafson BAS. Geminid meteoroids traced to cometary activity on Phaethon. A&A. 1989 Nov;225(2):533–540.
[198] Williams IP, Wu Z. The Geminid meteor stream and asteroid 3200 Phaethon. MNRAS. 1993 May;262(1):231–248.
[199] Jewitt D, Li J. Activity in Geminid parent (3200) Phaethon. AJ. 2010 Nov;140(5):1519–1527.
[200] Jewitt D, Li J, Agarwal J. The dust tail of asteroid (3200) Phaethon. ApJL. 2013 Jul;771(2):L36.
[201] Li J, Jewitt D. Recurrent Perihelion activity in (3200) Phaethon. AJ. 2013 Jun;145(6):154.
[202] Hui MT, Li J. Resurrection of (3200) Phaethon in 2016. AJ. 2017 Jan;153(1):23.
[203] Masiero JR, Davidsson BJR, Liu Y, et al. Volatility of sodium in carbonaceous chondrites at temperatures consistent with low-perihelion asteroids. Planet Sci J. 2021 Aug;2(4):165.
[204] Ansdell M, Meech KJ, Hainaut O, et al. Refined rotational period, pole solution, and shape model for (3200) Phaethon. ApJ. 2014 Sep;793(1):50.
[205] Nakano R, Hirabayashi M. Mass-shedding activities of asteroid (3200) Phaethon enhanced by its rotation. ApJL. 2020 Apr;892(2):L22.
[206] Hanuš J, Delbo' M, Vokrouhlický D, et al. Near-Earth asteroid (3200) Phaethon: characterization of its orbit, spin state, and thermophysical parameters. A&A. 2016 Jul;592:A34.
[207] Taylor PA, Rivera-Valentín EG, Benner LAM, et al. Arecibo radar observations of near-Earth asteroid (3200) Phaethon during the 2017 apparition. Planet Space Sci. 2019 Mar;167:1–8.
[208] Lauretta DS, Hergenrother CW, Chesley SR, et al. Episodes of particle ejection from the surface of the active asteroid (101,955) Bennu. Science. 2019 Dec;366(6470):eaay3544.
[209] Hergenrother CW, Maleszewski CK, Nolan MC, et al. The operational environment and rotational acceleration of asteroid (101,955) Bennu from OSIRIS-REx observations. Nat Commun. 2019 Mar;10:1291.
[210] Hergenrother CW, Maleszewski C, Li JY, et al. Photometry of particles ejected from active asteroid (101,955) Bennu. J Geophys Res (Planets). 2020 Sep;125(9):e06381.
[211] Bottke WF, Moorhead AV, Connolly HC, et al. Meteoroid impacts as a source of Bennu's particle ejection events. J Geophys Res (Planets). 2020 Aug;125(8):e06282.

[212] Molaro JL, Hergenrother CW, Chesley SR, et al. Thermal fatigue as a driving mechanism for activity on asteroid Bennu. J Geophys Res (Planets). 2020 Aug;125(8):e06325.
[213] Chesley SR, French AS, Davis AB, et al. Trajectory estimation for particles observed in the vicinity of (101,955) Bennu. J Geophys Res (Planets). 2020 Sep;125(9):e06363.
[214] Seligman DZ, Farnocchia D, Micheli M, et al. Dark comets? Unexpectedly large nongravitational accelerations on a sample of small asteroids. Planet Sci J. 2023 Feb;4(2):35.
[215] Chesley SR, Farnocchia D, Pravec P, et al. Direct detections of the Yarkovsky effect: status and outlook. In: Chesley SR, Morbidelli A, Jedicke R, et al., editors. Asteroids: new observations, new models; Vol. 318; Jan; 2016. p. 250–258.
[216] Farnocchia D, Seligman DZ, Granvik M, et al. (523,599) 2003 RM: the asteroid that wanted to be a comet. Planet Sci J. 2023 Feb;4(2):29.
[217] Hirabayashi M, Mimasu Y, Sakatani N, et al. Hayabusa2 extended mission: new voyage to rendezvous with a small asteroid rotating with a short period. Adv Space Res. 2021 Aug;68(3):1533–1555.
[218] Kameda S, Suzuki H, Cho Y, et al. Detectability of hydrous minerals using ONC-T camera onboard the Hayabusa2 spacecraft. Adv Space Res. 2015 Oct;56(7):1519–1524.
[219] Watanabe S, Tsuda Y, Yoshikawa M, et al. Hayabusa2 mission overview. Space Sci Rev. 2017 Jul;208(1–4):3–16.
[220] Arai T, Nakamura T, Tanaka S, et al. Thermal imaging performance of TIR onboard the Hayabusa2 spacecraft. Space Sci Rev. 2017 Jul;208(1–4):239–254.
[221] Okada T, Fukuhara T, Tanaka S, et al. Thermal infrared imaging experiments of C-type asteroid 162,173 Ryugu on Hayabusa2. Space Sci Rev. 2017 Jul;208(1–4):255–286.
[222] Takita J, Senshu H, Tanaka S. Feasibility and accuracy of thermophysical estimation of asteroid 162173 ryugu (1999 JU3) from the Hayabusa2 thermal infrared imager. Space Sci Rev. 2017 Jul;208(1–4):287–315.
[223] Mizuno T, Kase T, Shiina T, et al. Development of the laser altimeter (LIDAR) for Hayabusa2. Space Sci Rev. 2017 Jul;208(1–4):33–47.
[224] Senshu H, Oshigami S, Kobayashi M, et al. Dust detection mode of the Hayabusa2 LIDAR. Space Sci Rev. 2017 Jul;208(1–4):65–79.
[225] Yamada R, Senshu H, Namiki N, et al. Albedo observation by Hayabusa2 LIDAR: instrument performance and error evaluation. Space Sci Rev. 2017 Jul;208(1–4):49–64.
[226] Kameda S, Suzuki H, Takamatsu T, et al. Preflight calibration test results for optical navigation camera telescope (ONC-T) onboard the Hayabusa2 spacecraft. Space Sci Rev. 2017 Jul;208(1–4):17–31.
[227] Iwata T, Kitazato K, Abe M, et al. NIRS3: the near infrared spectrometer on Hayabusa2. Space Sci Rev. 2017 Jul;208(1–4):317–337.
[228] Suzuki H, Yamada M, Kouyama T, et al. Initial inflight calibration for Hayabusa2 optical navigation camera (ONC) for science observations of asteroid Ryugu. Icarus. 2018 Jan;300:341–359.
[229] Tatsumi E, Kouyama T, Suzuki H, et al. Updated inflight calibration of Hayabusa2's optical navigation camera (ONC) for scientific observations during the cruise phase. Icarus. 2019 Jun;325:153–195.
[230] Jewitt D, Hui MT, Kim Y, et al. The nucleus of interstellar comet 2I/Borisov. ApJL. 2020 Jan;888(2):L23.
[231] Jewitt D, Luu J. Initial characterization of interstellar comet 2I/2019 Q4 (Borisov). ApJL. 2019 Dec;886(2):L29.
[232] Bolin BT, Lisse CM, Kasliwal MM, et al. Characterization of the nucleus, morphology, and activity of interstellar comet 2I/Borisov by optical and near-infrared GROWTH, apache point, IRTF, ZTF, and keck observations. AJ. 2020 Jul;160(1):26.
[233] Guzik P, Drahus M, Rusek K, et al. Initial characterization of interstellar comet 2I/Borisov. Nat Astron. 2020 Jan;4:53–57.
[234] Hui MT, Ye QZ, Föhring D, et al. Physical characterization of interstellar comet 2I/2019 Q4 (Borisov). AJ. 2020 Aug;160(2):92.
[235] Mazzotta Epifani E, Dotto E, Perna D, et al. A colour portrait of the interstellar comet 2I/Borisov. Planet Space Sci. 2021 Nov;208:Article ID 105341.
[236] de León J, Licandro J, Serra-Ricart M, et al. Interstellar visitors: a physical characterization of comet C/2019 Q4 (Borisov) with OSIRIS at the 10.4 m GTC. Res Notes Am Astron Soc. 2019 Sep;3(9):131.
[237] de la Fuente Marcos C. Constraining the orientation of the spin axes of extrasolar minor bodies 1I/2017 U1 ('Oumuamua) and 2I/Borisov. A&A. 2020 Nov;643:A18.
[238] Manzini F, Oldani V, Ochner P, et al. Interstellar comet 2I/Borisov exhibits a structure similar to native Solar System comets. MNRAS. 2020 Jun;495(1):L92–L96.
[239] Yang B, Li A, Cordiner MA, et al. Compact pebbles and the evolution of volatiles in the interstellar comet 2i/borisov. Nat Astron. 2021. DOI:10.1038/s41550-021-01336-w
[240] Cremonese G, Fulle M, Cambianica P, et al. Dust environment model of the interstellar comet 2I/Borisov. ApJL. 2020 Apr;893(1):L12.
[241] Kim Y, Jewitt D, Mutchler M, et al. Coma anisotropy and the rotation pole of interstellar comet 2I/Borisov. ApJL. 2020 Jun;895(2):L34.
[242] Busarev VV, Petrova EV, Shcherbina MP, et al. Interstellar comet 2I/Borisov: dust composition from multiband photometry and modelling. MNRAS. 2021 Apr;502(2):1882–1894.
[243] Bagnulo S, Cellino A, Kolokolova L, et al. Unusual polarimetric properties for interstellar comet 2I/Borisov. Nat Commun. 2021 Jan;12:1797.
[244] Halder P, Sengupta S. A comprehensive model of morphologically realistic Cosmic Dust particles: an application to mimic the unusual Polarization properties of the interstellar comet 2I/Borisov. arXiv e-prints. Feb 2023. arXiv:2302.13370.
[245] Xing Z, Bodewits D, Noonan J, et al. Water production rates and activity of interstellar comet 2I/Borisov. ApJL. 2020 Apr;893(2):L48.
[246] Opitom C, Fitzsimmons A, Jehin E, et al. 2I/Borisov: A C_2-depleted interstellar comet. A&A. 2019 Nov;631:L8.
[247] McKay AJ, Cochran AL, Dello Russo N, et al. Detection of a water tracer in interstellar comet 2I/Borisov. ApJL. 2020 Jan;889(1):L10.

[248] Bodewits D, Noonan JW, Feldman PD, et al. The carbon monoxide-rich interstellar comet 2I/Borisov. Nat Astron. 2020 Apr;4:867–871.
[249] Cordiner MA, Milam SN, Biver N, et al. Unusually high CO abundance of the first active interstellar comet. Nat Astron. 2020 Apr;4:861–866.
[250] Fitzsimmons A, Hainaut O, Meech KJ, et al. Detection of CN gas in interstellar object 2I/Borisov. ApJL. 2019 Nov;885(1):L9.
[251] Kareta T, Andrews J, Noonan JW, et al. Carbon chain depletion of 2I/Borisov. ApJL. 2020 Feb;889(2):L38.
[252] Lin HW, Lee CH, Gerdes DW, et al. Detection of diatomic carbon in 2I/Borisov. ApJL. 2020 Feb;889(2):L30.
[253] Bannister MT, Opitom C, Fitzsimmons A, et al. Interstellar comet 2I/Borisov as seen by MUSE: C_2, NH_2 and red CN detections. arXiv e-prints. Jan 2020. arXiv:2001.11605.
[254] Aravind K, Ganesh S, Venkataramani K, et al. Activity of the first interstellar comet 2I/Borisov around perihelion: results from Indian observatories. MNRAS. 2021 Apr;502(3):3491–3499.
[255] Ye Q, Kelley MSP, Bolin BT, et al. Pre-discovery activity of new interstellar comet 2I/Borisov beyond 5 au. AJ. 2020 Feb;159(2):77.
[256] Lin HW, Lee CH, Gerdes DW, et al. Low resolution optical spectra and diatomic carbon detections of 2I/Borisov. arXiv e-prints. Dec 2019. arXiv:1912.06161.
[257] Guzik P, Drahus M. Gaseous atomic nickel in the coma of interstellar comet 2I/Borisov. Nature. 2021 May;593(7859):375–378.
[258] Preston GW. The spectrum of Ikeya-Seki (1965f). ApJ. 1967 Feb;147:718–742.
[259] Slaughter CD. The emission spectrum of comet Ikeya-Seki 1965-f at perihelion passage. AJ. 1969 Sep;74:929.
[260] Drahus M, Guzik P, Udalski A, et al. Multiple outbursts of interstellar comet 2I/Borisov. Astronomer's Tel. 2020 Mar;13549:1.
[261] Jewitt D, Kim Y, Mutchler M, et al. Outburst and splitting of interstellar comet 2I/Borisov. ApJL. 2020 Jun;896(2):L39.
[262] Jewitt D, Mutchler M, Kim Y, et al. Interstellar object 2I/Borisov double. Astronomer's Tel. 2020 Apr;13611:1.
[263] Bolin BT, Bodewits D, Lisse CM, et al. Possible fragmentation of interstellar comet 2I/Borisov. Astronomer's Tel. 2020 Apr;13613:1.
[264] Zhang Q, Ye Q, Kolokolova L. Interstellar comet 2I/Borisov is single again. Astronomer's Tel. 2020 Apr;13618:1.
[265] Brasser R, Wang JH. An updated estimate of the number of Jupiter-family comets using a simple fading law. A&A. 2015 Jan;573:A102.
[266] Price EM, Cleeves LI, Bodewits D, et al. Ice-coated pebble drift as a possible explanation for peculiar cometary CO/H_2O ratios. ApJ. 2021 May;913(1):9.
[267] Lisse CM, Gladstone GR, Young LA, et al. A predicted dearth of majority hypervolatile ices in oort cloud comets. Planet Sci J. 2022 May;3(5):112.
[268] Wierzchos K, Womack M. C/2016 R2 (PANSTARRS): a comet rich in CO and depleted in HCN. AJ. 2018 Jul;156(1):34.
[269] Cochran AL, McKay AJ. Strong CO^+ and N_2^+ emission in comet C/2016 R2 (Pan-STARRS). ApJL. 2018 Feb;854(1):L10.
[270] Mousis O, Aguichine A, Bouquet A, et al. Cold traps of hypervolatiles in the protosolar nebula at the origin of comet C/2016 R2 (PanSTARRS)'s peculiar composition. arXiv e-prints. Mar 2021. arXiv:2103.01793.
[271] Paganini L, Mumma MJ, Villanueva GL, et al. The chemical composition of CO-rich comet C/2009 p1 (Garradd) AT $R_h = 2.4$ and 2.0 AU before Perihelion. ApJL. 2012 Mar;748(1):L13.
[272] McKay AJ, Cochran AL, DiSanti MA, et al. Evolution of H_2O, CO, and CO_2 production in comet C/2009 P1 Garradd during the 2011–2012 apparition. Icarus. 2015 Apr;250:504–515.
[273] Feaga LM, A'Hearn MF, Farnham TL, et al. Uncorrelated volatile behavior during the 2011 apparition of comet C/2009 P1 Garradd. AJ. 2014 Jan;147(1):24.
[274] Bodewits D, Farnham TL, A'Hearn MF, et al. The evolving activity of the dynamically young comet c/2009 p1 (garradd). Astrophys J. 2014 Apr;786(1):48. DOI:10.1088/0004-637x/786/1/48
[275] Kawakita H, Dello Russo N, Vervack J R, et al. Extremely organic-rich coma of comet C/2010 G2 (Hill) during its outburst in 2012. ApJ. 2014 Jun;788(2):110.
[276] Biver N, Bockelée-Morvan D, Colom P, et al. The 1995 2002 long-term monitoring of comet C/1995 o1 (HALE BOPP) at radio wavelength. Earth Moon and Planets. 2002 Jun;90(1):5–14.
[277] Trilling DE, Robinson T, Roegge A, et al. Implications for planetary system formation from interstellar object 1I/2017 U1 ('Oumuamua). ApJL. 2017 Dec;850(2):L38.
[278] Laughlin G, Batygin K. On the consequences of the detection of an interstellar asteroid. Res Notes Am Astron Soc. 2017 Dec;1(1):43.
[279] Do A, Tucker MA, Tonry J. Interstellar interlopers: number density and origin of 'Oumuamua-like objects. ApJL. 2018 Mar;855:L10.
[280] Sekanina Z. A probability of encounter with interstellar comets and the likelihood of their existence. Icarus. 1976 Jan;27(1):123–133.
[281] McGlynn TA, Chapman RD. On the nondetection of extrasolar comets. ApJL. 1989 Nov;346:L105.
[282] Sen AK, Rana NC. On the missing interstellar comets. A&A. 1993 Aug;275:298.
[283] Jewitt D. Project pan-STARRS and the outer Solar System. Earth Moon Planets. 2003 Jun;92(1):465–476.
[284] Moro-Martın A, Turner EL, Loeb A. Will the large synoptic survey telescope detect extra-solar planetesimals entering the Solar System?. ApJ. 2009 Oct;704:733–742.
[285] Engelhardt T, Jedicke R, Vereš P, et al. An observational upper limit on the interstellar number density of asteroids and comets. AJ. 2017 Mar;153(3):133.
[286] Cook NV, Ragozzine D, Granvik M, et al. Realistic detectability of close interstellar comets. ApJ. 2016 Jul;825:51.
[287] Moro-Martín A. Origin of 1I/'Oumuamua. I. An ejected protoplanetary disk object?. ApJ. 2018 Oct;866(2):131.
[288] Moro-Martín A. Origin of 1I/'Oumuamua. II. An ejected exo-Oort cloud object?. AJ. 2019 Feb;157(2):86.

[289] Gomes R, Levison HF, Tsiganis K, et al. Origin of the cataclysmic late heavy bombardment period of the terrestrial planets. Nature. 2005 May;435(7041):466–469.
[290] Grav T, Mainzer AK, Bauer J, et al. WISE/NEOWISE observations of the jovian trojans: preliminary results. ApJ. 2011 Nov;742(1):40.
[291] Buie MW, Olkin CB, Merline WJ, et al. Size and shape from stellar occultation observations of the double Jupiter Trojan Patroclus and Menoetius. AJ. 2015 Mar;149(3):113.
[292] Nesvorný D, Vokrouhlický D, Bottke WF, et al. Evidence for very early migration of the Solar System planets from the Patroclus-Menoetius binary Jupiter Trojan. Nat Astron. 2018 Sep;2:878–882.
[293] Clement MS, Kaib NA, Raymond SN, et al. Mars' growth stunted by an early giant planet instability. Icarus. 2018 Sep;311:340–356.
[294] Clement MS, Kaib NA, Raymond SN, et al. The early instability scenario: terrestrial planet formation during the giant planet instability, and the effect of collisional fragmentation. Icarus. 2019 Mar;321:778–790.
[295] de Sousa RR, Morbidelli A, Raymond SN, et al. Dynamical evidence for an early giant planet instability. Icarus. 2020 Mar;339:Article ID 113605.
[296] Nesvorný D, Roig FV, Deienno R. The role of early giant-planet instability in terrestrial planet formation. AJ. 2021 Feb;161(2):50.
[297] Morgan M, Seligman D, Batygin K. Collisional growth within the Solar System's primordial planetesimal disk and the timing of the giant planet instability. ApJL. 2021 Aug;917(1):L8.
[298] Liu B, Raymond SN, Jacobson SA. Early Solar System instability triggered by dispersal of the gaseous disk. Nature. 2022 Apr;604(7907):643–646.
[299] Miret-Roig N, Bouy H, Raymond SN, et al. A rich population of free-floating planets in the upper scorpius young stellar association. Nat Astron. 2022 Jan;6:89–97.
[300] Jackson AP, Tamayo D, Hammond N, et al. Ejection of rocky and icy material from binary star systems: implications for the origin and composition of 1I/'Oumuamua. MNRAS. 2018 Jul;478(1):L49–L53.
[301] Ćuk M. 1I/'Oumuamua as a tidal disruption fragment from a binary star system. ApJL. 2018 Jan;852(1):L15.
[302] Childs AC, Martin RG. Misaligned circumbinary disks as efficient progenitors of interstellar asteroids. ApJL. 2022 Aug;935(2):L31.
[303] Hansen B, Zuckerman B. Ejection of material–'Jurads'–from post-main-sequence planetary systems. Res Notes Am Astron Soc. 2017 Dec;1(1):55.
[304] Rafikov RR. 1I/2017 'Oumuamua-like interstellar asteroids as possible messengers from dead stars. ApJ. 2018 Jul;861(1):35.
[305] Katz JI. Why is interstellar object 1I/2017 U1 ('Oumuamua) rocky, tumbling and possibly very prolate?. MNRAS. 2018 Jul;478(1):L95–L98.
[306] Pfalzner S, Aizpuru Vargas LL, Bhandare A, et al. Significant interstellar object production by close stellar flybys. A&A. 2021 Jul;651:A38.
[307] Veras D, Wyatt MC, Mustill AJ, et al. The great escape: how exoplanets and smaller bodies desert dying stars. MNRAS. 2011 Nov;417(3):2104–2123.
[308] Veras D, Tout CA. The great escape - II. Exoplanet ejection from dying multiple-star systems. MNRAS. 2012 May;422(2):1648–1664.
[309] Veras D, Evans NW, Wyatt MC, et al. The great escape – III. Placing post-main-sequence evolution of planetary and binary systems in a Galactic context. MNRAS. 2014 Jan;437(2):1127–1140.
[310] Wyatt MC, Bonsor A, Jackson AP, et al. How to design a planetary system for different scattering outcomes: giant impact sweet spot, maximising exocomets, scattered discs. MNRAS. 2017 Jan;464(3):3385–3407.
[311] Binney J, Merrifield M. Galactic astronomy. Princeton University Press; 1998.
[312] Binney J, Tremaine S. Galactic dynamics. 2nd ed. 2008.
[313] Holmberg J, Nordström B, Andersen J. The Geneva-Copenhagen survey of the solar neighbourhood. III. Improved distances, ages, and kinematics. A&A. 2009 Jul;501(3):941–947.
[314] Miville-Deschênes MA, Murray N, Lee EJ. Physical properties of molecular clouds for the entire milky way disk. ApJ. 2017 Jan;834(1):57.
[315] Schönrich R, Binney J, Asplund M. The detection and treatment of distance errors in kinematic analyses of stars. MNRAS. 2012 Feb;420(2):1281–1293.
[316] Robin AC, Bienaymé O, Fernández-Trincado JG, et al. Kinematics of the local disk from the RAVE survey and the Gaia first data release. A&A. 2017 Sep;605:A1.
[317] Mamajek E. Kinematics of the interstellar vagabond 1I/'Oumuamua (A/2017 U1). Res Notes Am Astron Soc. 2017 Dec;1(1):21.
[318] Gaidos E, Williams J, Kraus A. Origin of interstellar object A/2017 U1 in a nearby young stellar association?. RNAAS. 2017 Dec;1(1):13.
[319] Hallatt T, Wiegert P. The dynamics of interstellar asteroids and comets within the galaxy: an assessment of local candidate source regions for 1I/'Oumuamua and 2I/Borisov. AJ. 2020 Apr;159(4):147.
[320] Hsieh CH, Laughlin G, Arce HG. Evidence suggesting that 'Oumuamua is the 30 myr old product of a molecular cloud. ApJ. 2021 Aug;917(1):20.
[321] Dybczyński PA, Królikowska M. Investigating the dynamical history of the interstellar object 'Oumuamua. AAP. 2018 Feb;610:L11.
[322] Rivera EJ, Laughlin G, Butler RP, et al. The Lick-Carnegie exoplanet survey: a Uranus-Mass fourth planet for GJ 876 in an extrasolar laplace configuration. ApJ. 2010 Aug;719(1):890–899.
[323] Feng F, Jones HRA. 'Oumuamua as a messenger from the local association. ApJL. 2018 Jan;852(2):L27.
[324] Zuluaga JI, Sánchez-Hernández O, Sucerquia M, et al. A general method for assessing the origin of interstellar small bodies: the case of 1I/2017 U1 ('Oumuamua). AJ. 2018 Jun;155(6):236.
[325] Gaia Collaboration, Brown AGA, Vallenari A, et al. Gaia data release 1. Summary of the astrometric, photometric, and survey properties. A&A. 2016 Nov;595:A2.
[326] Zhang Q. Prospects for backtracing 1I/'Oumuamua and future interstellar objects. ApJL. 2018 Jan;852(1):L13.
[327] Bailer-Jones CAL, Farnocchia D, Meech KJ, et al. Plausible home stars of the interstellar object 'Oumuamua found in gaia DR2. AJ. 2018 Nov;156:205.

[328] Landgraf M, Grün E. In situ measurements of interstellar dust. In: Breitschwerdt D, Freyberg MJ, Truemper J, editors. Iau colloq. 166: the local bubble and beyond. Vol. 506; 1998. p. 381–384.
[329] Grün E, Landgraf M, Horányi M, et al. Techniques for galactic dust measurements in the heliosphere. J Geophys Res. 2000 May;105(A5):10403–10410.
[330] Grün E, Staubach P, Baguhl M, et al. South-North and radial traverses through the interplanetary dust cloud. Icarus. 1997 Oct;129(2):270–288.
[331] Grun E, Zook HA, Baguhl M, et al. Discovery of Jovian dust streams and interstellar grains by the Ulysses spacecraft. Nature. 1993 Apr;362(6419):428–430.
[332] Mathews JD, Meisel DD, Janches D, et al. Possible origins of low inclination antapex micrometeors observed using the Arecibo UHF radar. In: Baggaley WJ, Porubcan V, editors. Meteroids 1998; Jan.; 1999. p. 79.
[333] Meisel DD, Janches D, Mathews JD. Extrasolar micrometeors radiating from the vicinity of the local interstellar bubble. ApJ. 2002 Mar;567(1):323–341.
[334] Meisel DD, Janches D, Mathews JD. The size distribution of arecibo interstellar particles and its implications. ApJ. 2002 Nov;579(2):895–904.
[335] Baggaley WJ, Taylor AD, Steel DI. The influx of meteoroids with hyperbolic heliocentric orbits. In: Stohl J, Williams IP, editors. Meteoroids and their parent bodies; Jan.; 1993. p. 53.
[336] Baggaley WJ. Advanced Meteor Orbit Radar observations of interstellar meteoroids. J Geophys Res. 2000 May;105(A5):10353–10362.
[337] Taylor AD, Baggaley WJ, Steel DI. Discovery of interstellar dust entering the Earth's atmosphere. Nature. 1996 Mar;380(6572):323–325.
[338] Weryk RJ, Brown P. A search for interstellar meteoroids using the Canadian Meteor Orbit Radar (CMOR). Earth Moon Planets. 2004 Dec;95(1–4):221–227.
[339] Hawkes RL, Close T, Woodwoth S. Meteoroids from outside the solar system. In: Baggaley WJ, Porubcan V, editors. Meteroids 1998; Jan.; 1999. p. 257.
[340] Musci R, Weryk RJ, Brown P, et al. An optical survey for millimeter-sized interstellar meteoroids. ApJ. 2012 Feb;745(2):161.
[341] Hajduková JM. On the frequency of interstellar meteoroids. A&A. 1994 Aug;288:330–334.
[342] Hajduková JM, Paulech T. Interstellar and interplanetary meteoroid flux from updated IAU MDC data. In: Warmbein B, editor. Asteroids, comets, and meteors: ACM 2002; (ESA Special Publication; Vol. 500); Nov.; 2002. p. 173–176.
[343] Gould A, Jung YK, Hwang KH, et al. Free-Floating planets, the einstein desert, and 'OUMUAMUA. J Korean Astron Soc. 2022 Oct;55:173–194.
[344] Wiegert PA. Hyperbolic meteors: interstellar or generated locally via the gravitational slingshot effect?. Icarus. 2014 Nov;242:112–121.
[345] Higuchi A, Kokubo E. Hyperbolic orbits in the Solar System: interstellar origin or perturbed oort cloud comets?. MNRAS. 2020 Feb;492(1):268–275.
[346] Hajdukova M, Sterken V, Wiegert P, et al. The challenge of identifying interstellar meteors. Planet Space Sci. 2020 Nov;192:Article ID 105060.
[347] Peña-Asensio E, Trigo-Rodríguez JM, Rimola A. Orbital characterization of superbolides observed from space: dynamical association with near-Earth objects, meteoroid streams, and identification of hyperbolic meteoroids. AJ. 2022 Sep;164(3):76.
[348] Siraj A, Loeb A. A meteor of apparent interstellar origin in the CNEOS fireball catalog. ApJ. 2022 Nov;939(1):53.
[349] Devillepoix HAR, Bland PA, Sansom EK, et al. Observation of metre-scale impactors by the desert fireball network. MNRAS. 2019 Mar;483(4):5166–5178.
[350] Vaubaillon J. Hyperbolic meteors: is CNEOS 2014-01-08 interstellar?. WGN J Int Meteor Org. 2022;50(5):140–143.
[351] Levison HF, Duncan MJ, Brasser R, et al. Capture of the Sun's Oort cloud from stars in its birth cluster. Science. 2010 Jun;329(5988):187–190.
[352] Peñarrubia J. A halo of trapped interstellar matter surrounding the Solar System. MNRAS. 2023 Feb;519(2):1955–1980.
[353] Napier KJ, Adams FC, Batygin K. On the capture of interstellar objects by our Solar System. Planet Sci J. 2021 Apr;2(2):53.
[354] Dehnen W, Hands TO. Capture of interstellar objects – I. The capture cross-section. MNRAS. 2022 May;512(3):4062–4077.
[355] Napier KJ, Adams FC, Batygin K. On the fate of interstellar objects captured by our Solar System. Planet Sci J. 2021 Dec;2(6):217.
[356] Namouni F, Morais MHM. An interstellar origin for high-inclination Centaurs. MNRAS. 2020 May;494(2):2191–2199.
[357] Morbidelli A, Batygin K, Brasser R, et al. No evidence for interstellar planetesimals trapped in the Solar System. MNRAS. 2020 Sep;497(1):L46–L49.
[358] Weidenschilling SJ. Aerodynamics of solid bodies in the solar nebula. MNRAS. 1977 Jul;180:57–70.
[359] Weidenschilling SJ. Dust to planetesimals: settling and coagulation in the solar nebula. Icarus. 1980 Oct;44(1):172–189.
[360] Zsom A, Ormel CW, Güttler C, et al. The outcome of protoplanetary dust growth: pebbles, boulders, or planetesimals? II. Introducing the bouncing barrier. A&A. 2010 Apr;513:A57.
[361] Youdin AN, Goodman J. Streaming instabilities in protoplanetary disks. ApJ. 2005 Feb;620(1):459–469.
[362] Youdin AN, Shu FH. Planetesimal formation by gravitational instability. ApJ. 2002 Nov;580(1):494–505.
[363] Windmark F, Birnstiel T, Ormel CW, et al. Breaking through: the effects of a velocity distribution on barriers to dust growth. A&A. 2012 Aug;544:L16.
[364] Johansen A, Andersen AC, Brandenburg A. Simulations of dust-trapping vortices in protoplanetary discs. A&A. 2004 Apr;417:361–374.
[365] Okuzumi S, Tanaka H, Sakagami M. Numerical modeling of the coagulation and porosity evolution of dust aggregates. ApJ. 2009 Dec;707(2):1247–1263.
[366] Okuzumi S. Electric charging of dust aggregates and its effect on dust coagulation in protoplanetary disks. ApJ. 2009 Jun;698(2):1122–1135.
[367] Pfalzner S, Bannister MT. A hypothesis for the rapid formation of planets. ApJL. 2019 Apr;874(2):L34.

[368] Pfalzner S, Paterson D, Bannister MT, et al. Interstellar objects follow the collapse of molecular clouds. ApJ. 2021 Nov;921(2):168.
[369] Grishin E, Perets HB, Avni Y. Planet seeding through gas-assisted capture of interstellar objects. MNRAS. 2019 Aug;487(3):3324–3332.
[370] Moro-Martín A, Norman C. Interstellar planetesimals: potential seeds for planet formation?. ApJ. 2022 Jan; 924(2):96.
[371] Seligman D, Laughlin G. The feasibility and benefits of in situ exploration of 'Oumuamua-like objects. AJ. 2018 May;155(5):217.
[372] Hoover DJ, Seligman DZ, Payne MJ. The population of interstellar objects detectable with the LSST and accessible for in situ rendezvous with various mission designs. Planet Sci J. 2022 Mar;3(3):71.
[373] Marčeta D. Synthetic population of interstellar objects in the Solar System. Astron Comput. 2023 Jan;42:Article ID 100690.
[374] Jones RL, Chesley SR, Connolly AJ, et al. Solar System science with LSST. Earth Moon Planets. 2009 Sep;105(2-4):101–105.
[375] Ivezić Ž, Kahn SM, Tyson JA, et al. LSST: from science drivers to reference design and anticipated data products. ApJ. 2019 Mar;873(2):111.
[376] Solontoi M, Ivezić Ž, Jones L. Comet science with lsst. In: American astronomical society meeting abstracts# 217; Vol. 217; 2011. p. 252–211.
[377] Vereš P, Chesley SR. Near-earth object orbit linking with the large synoptic survey telescope. AJ. 2017 Jul;154(1):13.
[378] Vereš P, Chesley SR. High-fidelity simulations of the near-Earth object search performance of the large synoptic survey telescope. AJ. 2017 Jul;154(1):12.
[379] Jones RL, Slater CT, Moeyens J, et al. The large synoptic survey telescope as a near-Earth object discovery machine. Icarus. 2018 Mar;303:181–202.
[380] Mainzer A, Grav T, Bauer J, et al. Survey simulations of a new near-Earth asteroid detection system. AJ. 2015 May;149(5):172.
[381] Jones G. ESA comet interceptor team: comet interceptor a mission to a dynamically new solar system object; 2019. Available from: http://www.cometinterceptor.space.
[382] Hein AM, Perakis N, Eubanks TM, et al. Project Lyra: sending a spacecraft to 1I/'Oumuamua (former A/2017 U1), the interstellar asteroid. arXiv e-prints. Nov 2017. arXiv:1711.03155.
[383] Meech K, Castillo-Rogez J, Hainaut O, et al. Sampling extrasolar planetary systems: interstellar objects in the Solar System. BAAS. 2019 May;51(3):552.
[384] Castillo-Rogez J, Landau D, Chung SJ, et al. In: Approach to exploring interstellar objects and long-period comets; 01; 2019.
[385] Hibberd A, Hein AM, Eubanks TM. Project lyra: catching 1I/'Oumuamua – mission opportunities after 2024. Acta Astronaut. 2020 May;170:136–144.
[386] Linares R, Landau D, Miller D, et al. Rendezvous mission for interstellar objects using a solar sail-based statite concept. arXiv e-prints. 2020 Dec. arXiv:2012.12935.
[387] Donitz BP, Castillo-Rogez JC, Matousek SE. Rapid response to long period comets and interstellar objects using smallsat architecture. In: 2021 IEEE Aerospace Conference (50100); 2021. p. 1–12.
[388] Pau Sánchez J, Morante D, Hermosin P, et al. ESA F-class comet interceptor: trajectory design to intercept a yet-to-be-discovered comet. arXiv e-prints. Jul 2021. arXiv:2107.12999.
[389] Meech K, Castillo-Rogez J, Bufanda E, et al. In-situ exploration of objects on oort cloud comet orbits: OCCs, Manxes and ISOs. In: Bulletin of the american astronomical society; Vol. 53; May; 2021. p. 282.
[390] Hibberd A, Hein A, Eubanks M, et al. Project Lyra: A mission to 1I/'Oumuamua without solar oberth manoeuvre. arXiv e-prints. Jan 2022. arXiv:2201.04240.
[391] Moore K, Castillo-Rogez J, Meech KJ, et al. Rapid response missions to explore fast, high-Value targets such as interstellar objects and long period comets. Bull Am Astron Soc. 2021 May;53:481.
[392] Moore K, Courville S, Ferguson S, et al. Bridge to the stars: A mission concept to an interstellar object. Planet Space Sci. 2021 Mar;197:Article ID 105137.
[393] Hein AM, Eubanks TM, Lingam M, et al. Interstellar now! missions to explore nearby interstellar objects. Adv Space Res. 2022 Jan;69(1):402–414.
[394] Mages D, Landau D, Donitz B, et al. Navigation evaluation for fast interstellar object flybys. Acta Astronaut. 2022 Feb;191:359–373.
[395] Miller D, Duvigneaud F, Menken W, et al. High-performance solar sails for interstellar object rendezvous. Acta Astronaut. 2022 Nov;200:242–252.
[396] Garber D, Friedman LD, Davoyan A, et al. A fast response mission to rendezvous with an interstellar object. Exp Astron. 2022 Jun;53(3):945–960.